GeoStorage

Vol. 2, No. 1, p. 78-97, 2026

Research article

# Experimental and Numerical Study on the Mechanical Evolution of Shizhu Shale under Water-rock Interaction

Bao Li[1,2,3], Yongjian Zhu[1], Yizhen Li[4], Yafei Luo[1]*, Yintong Guo[2,3], Mingyang Wu[2,3]

[1] *School of Resource & Environment and Safety Engineering, Hunan University of Science and Technology, Xiangtan 411201, China*
[2] *State Key Laboratory of Geomechanics and Geotechnical Engineering Safety, Institute of Rock and Soil Mechanics, Chinese Academy of Sciences, Wuhan 430071, China*
[3] *University of Chinese Academy of Sciences, Beijing 100049, China*
[4] *CNPC Chuanqing Drilling Engineering Company Limited, Chengdu 610056, China*

**Keywords:**
Shale
water-rock interaction
mechanical properties
mineral composition
fractal dimension

**Cited as:**
Li B, Zhu YJ, Li YZ, et al. 2026. Experimental and Numerical Study on the Mechanical Evolution of Shizhu Shale under Water-rock Interaction. *GeoStorage*, 2(1), 78-97.
https://doi.org/10.46690/gs.2026.01.06

**Abstract:**
To investigate the mechanical degradation characteristics and underlying mechanisms of Shizhu shale under water-rock interaction, this study combines laboratory experiments with numerical simulations. Shale specimens are immersed in field-produced water for 0, 1, 3, 7, 15, and 30 days, followed by X-ray diffraction (XRD) mineralogical analysis, Brazilian tensile tests, and triaxial compression tests. Based on the finite- discrete element method (FDEM), a numerical model incorporating mineralogical evolution is established to verify and analyze the influence mechanisms of mineral components on the mechanical behavior of shale. XRD results indicate that under flowback fluid immersion, carbonate minerals such as dolomite and calcite exhibit pronounced fluctuations characterized by a dynamic dissolution - precipitation process, whereas quartz shows strong chemical inertness and clay minerals (illite) display only minor variations. The mechanical properties of shale show a pronounced time - dependent evolution. The Brazilian tensile strength exhibits a fluctuating trend of slight decrease - recovery - slight decrease, while the triaxial compressive strength evolves through three stages: strengthening (0 - 3 days), degradation (7 - 15 days), and re-stabilization (15 - 30 days). The peak compressive strength increases from an initial value of 346.54 MPa to 402.99 MPa at 3 days, decreases to 164.27 MPa at 7 days, and finally stabilizes at 174. 22 MPa at 30 days. Failure patterns evolve with soaking time, which is closely coupled with mineralogical variation and microstructural reconstruction. The established FDEM model reproduces the mechanical responses and failure patterns of shale, confirming that the macroscopic mechanical behavior of shale results from a dynamic balance between the strengthening effects of hard minerals (dolomite and quartz) and the weakening effects of soft minerals (illite and calcite). This study can provide theoretical references for integrity assessment and risk control of underground oil and natural gas storage.

## 1 Introduction

Underground storage of oil and natural gas is a cornerstone technology for energy security, seasonal peak shaving, and emergency supply (Guo et al., 2022; Al-Shafi et al., 2023; Liu et al., 2025). Storage is commonly implemented in depleted hydrocarbon reservoirs, aquifers, and salt caverns, where repeated injection and withdrawal cause cyclic variations in pore pressure and effective stress. Such cyclic hydro-chemo-mechanical disturbances may progressively modify the mineral composition, pore structure, and mechanical integrity of the host rock and sealing formations, thereby affecting containment reliability, injectivity/withdrawal performance, and long-term operational safety (Mao et al., 2025; Song et al., 2026). A key issue is the sustained contact between formation fluids (produced water/brine) and the rock matrix during cycling and shut-in periods. These water-rock interactions can trigger mineral

Yandy Scientific Press

* Corresponding author.
*E-mail address*: li946187831@163.com (Li B); lin13659864130@163.com (Zhu YJ); liyzh_dyy@cnpc.com.cn (Li YZ); luoyafei@cqu.edu.cn (Luo YF); ytguo@whrsm.ac.cn (Guo YT); mywu@whrsm.ac.cn (Wu MY)

Received Feb. 28, 2026; revised Mar. 15, 2025; accepted Mar. 18, 2026; available online Mar. 19, 2026.

dissolution/precipitation, clay swelling and ion exchange, and subcritical crack growth (Zou et al., 2024), ultimately altering strength, stiffness, and failure mode (Bourg et al., 2017; Lyu et al., 2018; Chen et al., 2019). Therefore, clarifying the time-dependent mechanical degradation mechanism of shale under representative storage-fluid environments is crucial for designing and managing underground oil and gas storage facilities.

The contact between fluid and reservoir rock triggers chemical reactions between the fluid and the rock, leading to the accumulation of hydraulic mechanical damage. During processes such as cushion gas injection, cyclic recovery, and periodic well intervention, fluid and saline water may enter fractures and pores, promoting chemical reactions and the accumulation of hydraulic mechanical damage. In recent years, the interaction between water and rock, as well as the weakening effect of water on underground reservoirs and sealing rocks, has garnered increasing attention. Previous studies demonstrate that such interactions directly affect the pore structure and mechanical properties of shale and other clay-bearing rocks (Chen et al., 2014; Shen et al., 2019; Pang et al., 2025). Experimental investigations using nuclear magnetic resonance (NMR) and scanning electron microscope (SEM) reveal that water-rock reactions enlarge pores and alter pore connectivity, thereby significantly modifying petrophysical properties (Cai et al., 2019). Li et al. through triaxial tests show that, under the same confining pressure, the triaxial compressive strength of clay-bearing rocks decreases markedly with increasing water content, indicating substantial strength degradation induced by hydration (Li et al., 2025). Meanwhile, increasing water content also drives a transition in failure mode from brittle to ductile behavior, making shear bands and viscous deformation more likely to develop. The degradation of macroscopic mechanical properties is attributed to underlying microscopic processes. Water absorption and swelling of clay minerals, together with the disintegration of cementing materials, loosen particle contacts and weaken inter-granular bonding. Simultaneously, pore water pressure reduces effective stress, further exacerbating strength deterioration. Natural fractures and mineralogical heterogeneity are inherent characteristics of shale, and their combined effects govern the mechanical response under water-rock interaction.

In the process of water rock interaction, the mechanical degradation of rocks is complex and easily affected by mineral changes. Due to the evolution of fractures influenced by minerals is difficult to observe solely through physical experiments, numerical simulation becomes an important means of studying the changes in mechanical properties under the influence of minerals. The finite-discrete element method (FDEM) is capable of simultaneously simulating the continuous deformation and fracture behavior of rock materials, making it a powerful tool for investigating crack initiation and interfacial mechanics (Fukuda et al., 2021; Chen et al., 2023a). In FDEM, cohesive elements with defined stiffness and failure criteria are embedded between finite element meshes, allowing cracks to initiate randomly, propagate, and naturally form complex fracture networks (Erguler et al., 2009; Sun et al., 2020; Xia et al., 2024). Therefore, compared with conventional finite element methods (FEM), FDEM is a more effective method for simulating heterogeneity and capturing fracture discontinuities in rock samples (Deng et al., 2024). As a result, the simulation study of rock mechanical properties under mineral influence based on FDEM has received increasing attention. Li et al. apply FDEM to Brazilian splitting tests on Weiyuan shale and demonstrate that variations in mineral composition significantly influence fracture behavior. Overall, by embedding cohesive elements, FDEM effectively characterizes crack initiation and propagation and enables the simulation of complex fracture network development in heterogeneous rock masses. These capabilities provide distinct advantages for investigating fracture evolution, interfacial mechanical behavior, and mineralogical heterogeneity under water-rock interaction.

Rock fracture surfaces and fracture networks often exhibit self-similar geometric characteristics, and fractal dimension is commonly used to quantitatively describe their complexity and roughness. Fractal dimension serves as an effective parameter for characterizing fracture roughness and the distribution patterns of fragmented debris, with higher values indicating more complex and rougher fracture geometries (Lai et al., 2018). Fractal analysis is widely applied in unconventional rock mechanics to quantify the morphology of fracture networks and the irregularity of failure surfaces, providing an important tool for understanding complex fracture systems. Among various approaches, the box-counting method is commonly employed to estimate the fractional dimension of the space occupied by fractures or fragmented surfaces. Previous studies indicate that the fractal dimension of fracture surfaces or rock fragments is closely related to material toughness: rocks with higher toughness tend to develop rougher failure surfaces and exhibit larger fractal dimensions (Wu et al., 2021). Therefore, quantitatively characterizing rock fracture features through fractal dimension is one of the objective methods.

This study focuses on the outcrop shale in Shizhu County, Chongqing. Field-collected produced water is used as the soaking medium, and both laboratory experiments and numerical simulations are employed to simulate the water-rock interaction environment during the shut-in period. Firstly, the introduction to the soaking experiment, X-ray diffraction (XRD) analysis, Brazilian splitting test, triaxial compression test, and the FDEM method is presented in Section 2. The results of the laboratory tests are presented in Section 3. Subsequently, the changes in the simulation results of Brazilian splitting and triaxial compression under the influence of mineral changes in water-rock reactions and a comprehensive discussion are presented in Section 4. The conclusions are provided in Section 5.

## 2 Methodologies

To investigate the mechanical mechanism of shale under water-rock interactions, the sampling and processing standards for columnar shale are presented in Section 2.1. Then, the soaking test protocol and laboratory tests, including X-ray diffraction (XRD), Brazilian splitting test, and triaxial compression test, are described in Section 2.2. The FDEM method for constructing Brazilian splitting and triaxial compression simulation models considering the influence of mineral composition changes is introduced in Section 2.3

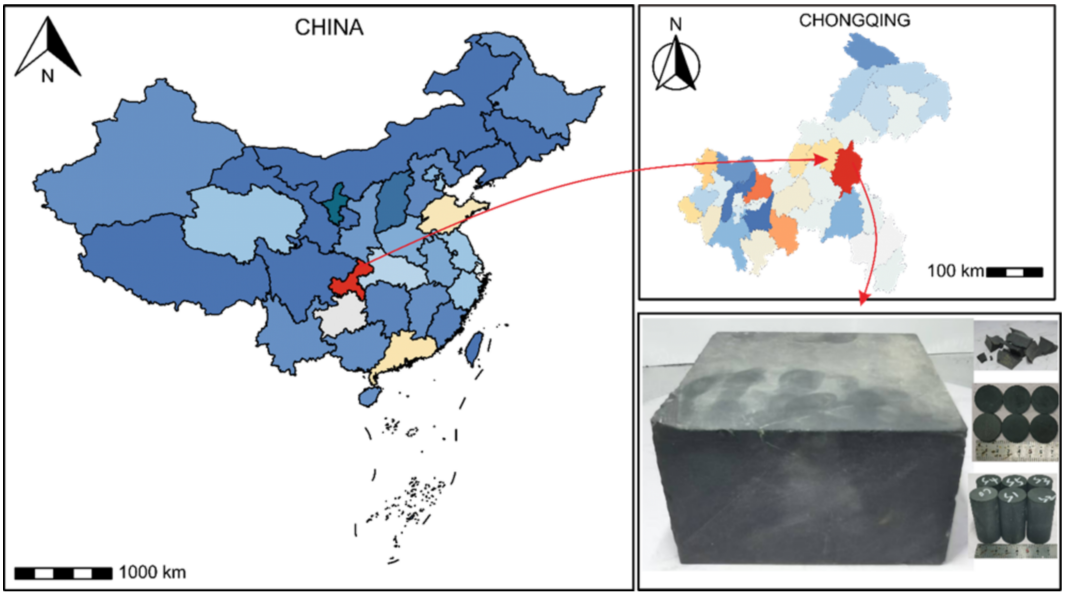


**Fig. 1** Schematic diagram of shale directional coring

## 2.1 Sample preparation

The experimental shale samples are collected from outcrops in Shizhu County, Chongqing. To minimize the influence of variations in mineral composition, bedding, and other factors on experimental results, all specimens are processed from the same rock slab. Six cylindrical specimens with dimensions of $\phi 25mm \times 50mm$ are prepared for triaxial compression tests. Six-disc specimens with dimensions of $\phi 25mm \times 12.5mm$ are prepared for Brazilian splitting tests. All sample preparation strictly follows international rock mechanics testing standards, with end-face parallelism controlled within $\pm 0.02mm$. Material of similar quality from the remaining processed rock is selected for XRD analysis of mineral composition (Fig.1).

## 2.2 Experimental design

To better reproduce the time-dependent effects of shale-fluid interaction relevant to underground gas storage operations, the experiments use field-collected produced water/flowback fluid as the soaking medium. The prepared shale specimens are divided into six groups: the first group is the original, un-soaked specimens, while the remaining five groups are soaked for 1, 3, 7, 15, and 30 days, respectively. The procedure is as follows: The shale specimens are first oven-dried, and their mass is measured and recorded. Under constant temperature conditions, specimens of each group are placed in sealed beakers for soaking. After reaching the preset soaking duration, the specimens are removed, cleaned, and wrapped in cling film for subsequent experimental testing.

To accurately record morphological changes of Shizhu shale under soaking, a custom-developed 3D imaging system is used to capture the surface morphology of $\phi 25mm \times 50mm$ specimens from multiple angles before and after soaking. Photographs from different angles are combined to construct a 3D model, reproducing the surface morphology of the shale in a one-to-one ratio and enabling direct observation of morphological changes due to soaking.

XRD Analysis: Mineral composition of shale before and after soaking is analyzed using a Bruker AXS D8-Focus X-ray diffractometer (Germany). Specimens with similar mass before and after soaking are ground and passed through a 200-mesh sieve. The powdered samples are uniformly loaded into the XRD sample holder, using an appropriate base or pressing method to ensure homogeneity. The XRD instrument is then operated to scan the samples, and the diffraction data are recorded. Analysis of the resulting diffraction patterns allows identification of different mineral components and their relative contents. Brazilian Splitting Test: The Brazilian splitting tests are conducted using an RMT-150C multifunctional rock mechanics testing system developed by the Institute of Rock and Soil Mechanics, Chinese Academy of Sciences, Wuhan. Disc specimens with dimensions of $\phi 25mm \times 12.5mm$ are loaded under the lower square loading jaws using a displacement-controlled mode at a constant rate of 0.002 $mm/s$ until splitting failure occurs. Stress-displacement curves are recorded, and the specimen failure morphology is photographed. Triaxial Compression Test: Triaxial compression tests are performed using an MTS815.03 rock testing frame (MTS Systems, USA). Cylindrical specimens with dimensions of $\phi 25mm \times 50mm$ are loaded under room temperature. The confining pressure is applied at a rate of 0.05 $kN/s$ until reaching 60 MPa and maintained for 120 $s$. Axial loading is then applied in displacement-controlled mode at a rate of 0.001 $m/s$ until specimen failure.

## 2.3 Simulation method

To investigate the influence of mineral composition on the mechanical properties of Shizhu shale, a numerical simulation model for Brazilian splitting and triaxial compression considering mineral components is constructed based on FDEM. During model construction, the shale material was initially divided into a finite number of discrete elements. Zero-thickness cohesive elements are placed at the interfaces between adjacent elements, forming a composite material model that combines discrete

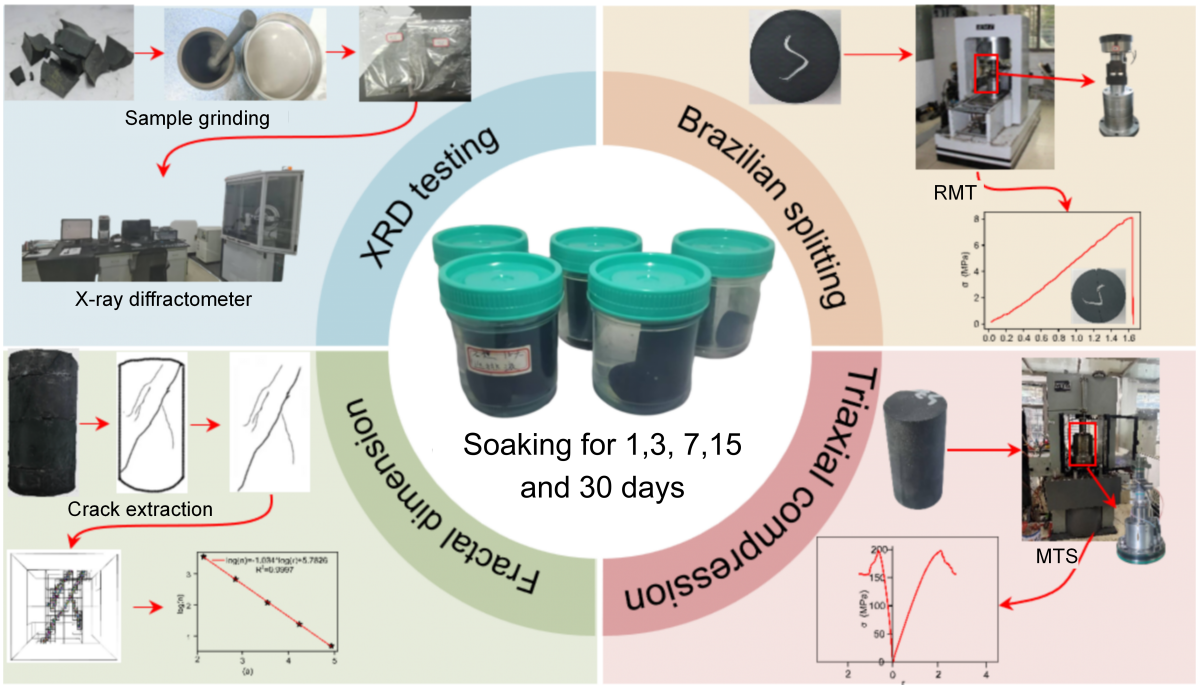


**Fig. 2** Comprehensive test program

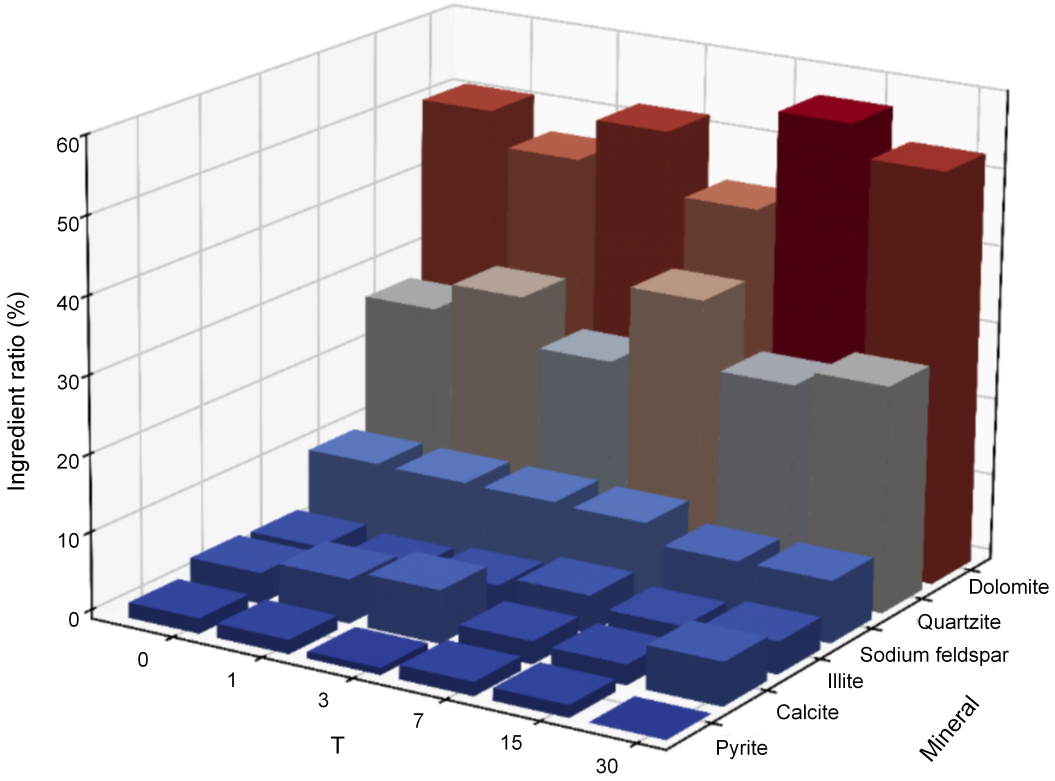


**Fig. 3** Variation of mineral components in shale subjected to prolonged soaking

elements and cohesive elements. The zero-thickness cohesive elements are used to characterize the contact interaction mechanism at the boundaries of mineral discrete elements. The cohesive properties of the cohesive elements are used to represent the initiation and propagation of cracks.

The failure of the cohesive elements directly reflects the crack development process. As demonstrated by Zheng et al., the "relative displacement-stress" criterion effectively captures this type of interaction (Zheng et al., 2023). In this study, the traction-separation model is used to define the intrinsic behavior of the cohesive elements. Prior to damage initiation, the deformation of the cohesive elements is governed by the

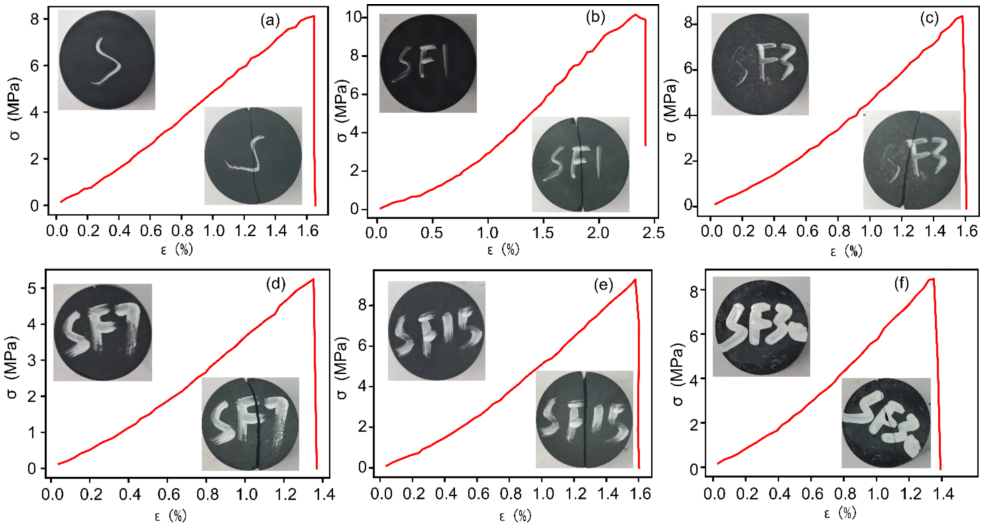


**Fig. 4** Brazilian splitting stress-strain and fracture morphology of different soaking times ((a):0 day; (b):1 day; (c):3 day; (d):7 day; (e):15 day; (f):30 day)

traction-separation law, which follows a linear-elastic relationship. The stress-strain behavior of the material in the linear-elastic phase, before damage evolution, is described by the following equations:

The cohesive elements along the crack propagation path adhere to the traction-separation law. To balance computational efficiency and result accuracy, the bilinear model (Li, 2023; Zhang et al., 2024) is applied to the traction-separation law:

Before damage, the deformation behavior of the cohesive element is governed by the law of traction separation, which satisfies the linear elasticity relation.

$$t = \begin{Bmatrix} t_n \\ t_s \\ t_t \end{Bmatrix} = \begin{bmatrix} K_m & K_{ns} & K_{nt} \\ K_{ns} & K_{ss} & K_{st} \\ K_{nt} & K_{st} & K_{tt} \end{bmatrix} \begin{Bmatrix} \varepsilon_n \\ \varepsilon_s \\ \varepsilon_t \end{Bmatrix} = K\varepsilon \tag{1}$$

where $\varepsilon_n = \delta_n/T_0$, $\varepsilon_s = \delta_s/T_0$, $\varepsilon_t = \delta_t/T_0$. $\varepsilon_n$ is the strain in the normal direction; $\varepsilon_s, \varepsilon_t$ are the strains in the two transverse shear directions; $T_0$ is the initial thickness of the interfacial element, $m$; $\delta_n$ is the normal tensile displacement, $m$; $\delta_s, \delta_t$ are the tensile displacements in the two transverse shear directions, $m$.

The quads damage criterion is used to determine the fracture of the cohesive element, which can be expressed as:

$$\left(\frac{\langle T_n \rangle}{T_n^0}\right)^2 + \left(\frac{T_s}{T_s^0}\right)^2 + \left(\frac{T_t}{T_t^0}\right)^2 = 1 \tag{2}$$

where $T_n$, $T_s$, and $T_t$ are the normal and the two tangential tractions of the cohesive element, respectively; $T_n^0$, $T_s^0$, and $T_t^0$ are their corresponding peaks; and $\langle\ \rangle$ is the McCauley bracket that distinguishes between the cohesive element in compression ($T_n < 0$) and in tension ($T_n \geq 0$). When the cohesive element is not damaged ($D = 0$), the traction in each direction increases linearly with relative displacement. When the traction force in each direction of the cohesive element satisfies the Quads damage criterion, the cohesive element enters the damage evolution phase.

In the numerical simulation study, the displacement damage evolution criterion is mainly used, and the cohesive elements are designed to fail in tensile and shear modes following the bilinear traction separation criterion. The crack extension process can be determined by observing the numerical changes in the damage factor (Dahi Taleghani et al., 2016) to determine whether a new crack is created.

$$\sigma_n = \begin{cases} (1-D)\overline{\sigma}_n, \overline{\sigma}_n \geq 0 \\ \overline{\sigma}_n, \text{compress} \end{cases} \tag{3}$$

$$\sigma_s = (1-D)\overline{\sigma_s} \tag{4}$$

$$\sigma_t = (1-D)\overline{\sigma_t} \tag{5}$$

where $\overline{\sigma_n}$ denotes the stress in the normal direction of the cohesive element at the current strain predicted by the elastic traction-separation criterion of the undamaged line, MPa; $\overline{\sigma_s}, \overline{\sigma_t}$ denote the shear stresses in the two transverse directions of the cohesive element at the current strain predicted by the elastic traction-separation criterion of the undamaged line, MPa; $\sigma_n, \sigma_s, \sigma_t$ are the corresponding three directions of the actual stresses, MPa.

The damage factor in the stiffness degradation criterion (Dahi Taleghani et al., 2018) is when the linear displacement expansion criterion is used:

$$D = \frac{d_m^f(d_m^{\max} - d_m^0)}{d_m^{\max}(d_m^f - d_m^0)} \tag{6}$$

where $d_m^{\max}$ is the maximum displacement value of the element when loading, $m$; $d_m^f$ is the displacement value of the elements when it is completely damaged, $m$; $d_m^0$ is the displacement value of the elements when it is initially damaged, $m$.

The damage factor in the stiffness degradation criterion when using the nonlinear displacement expansion criterion is used:

$$D = 1 - \left\{ \frac{d_m^0}{d_m^{\max}} \right\} \left\{ 1 - \frac{1 - \exp\left( -\beta \left( \frac{d_m^{\max} - d_m^0}{d_m^0 - d_m^0} \right) \right)}{1 - \exp(-\beta)} \right\} \tag{7}$$

where $\beta$ is an index describing the rate of crack expansion. The damage variable $D$ follows the evolutionary rule.

$$D = \begin{cases} 0, & S < S_0 \\ 1 - \frac{S_0}{S} \cdot \left( 1 - \frac{S - S_0}{S_m - S_0} \right), & S \geq S_0 \end{cases} \tag{8}$$

where $S_0$ and $S_m$ are the relative displacements at which the cohesive element begins to damage and completely breaks, respectively.

$$T = (1 - D)KS \tag{9}$$

where $T$ is the traction force; $D$ is the damage variable; $K$ is the initial stiffness; $S$ is the relative displacement.

## 3 Experimental results and analysis

The mineral composition within rock undergoes certain chemical reactions under the influence of backflow immersion, thereby affecting the rock's mechanical properties. To investigate the mechanical evolution of shale columns under water-rock interaction, a mineralogical analysis of the shale under varying immersion durations is presented in Section 3.1. Subsequently, the Brazilian splitting tensile strength properties of the shale are examined under different immersion periods is presented in Section 3.2, and the triaxial compression failure characteristics of the rock under varying immersion durations are analyzed in Section 3.3. Finally, a quantitative analysis of the cracks in the damaged Brazilian split and triaxial compression specimens was conducted, which is presented in Section 3.4.

### 3.1 Variation of mineral components

Fig.3 shows the variation in mineral component content of different soaking times. Obviously, the Shizhu shale composition primarily comprises three categories: clay minerals (illite), carbonate minerals (dolomite, calcite), silicate minerals (quartz, sodium feldspar), and other minerals (pyrite). Meanwhile, the mineral composition ratio of dolomite and quartz is the highest, followed by albite, illite, and calcite, while the abundance of pyrite is the lowest. Notably, the soaking duration exerts differentiated effects on various minerals. Minerals with high abundance (exceeding 40%), such as dolomite and calcite, exhibit the most significant fluctuations in content. Although the influence of soaking time varies among minerals with different abundances, all minerals display a trend of rapid changes during both the early and late stages of soaking. The dolomite content shows intense fluctuations with increasing soaking time, whereas the variation pattern of quartz presents an alternating "rise-and-fall" dynamic response relative to dolomite. This indicates that the soaking process plays a strong regulatory role in mineral dissolution/precipitation and component migration. These phenomena are likely attributed to the combined effects of differences in mineral dissolution kinetics, the chemical evolution of the solution, and mineral-fluid interactions (Zhang et al., 2007; Liu et al., 2024). Quartz, as a silicate mineral, undergoes a dissolution reaction with extremely high mechanical stability, and only exhibits slight dissolution under high-temperature or strongly alkaline conditions, reflecting its strong chemical inertness (Wilson, 2020).

However, due to limitations of the experimental apparatus, the specific mechanisms underlying the variations among mineral components of the Shizhu shale during soaking in produced water remain difficult to elucidate. Nevertheless, based on the observed variation patterns of mineral compositions under different soaking durations, it is evident that the changes in mineral components of the Shizhu shale are strongly influenced by soaking time.

### 3.2 Variation in mechanical properties under Brazilian splitting

Fig.4 presents the brazilian splitting stress-strain and fracture morphology of different soaking times. The macroscopic mechanical response and fracture patterns of shale exhibit pronounced time-dependent degradation, which is essentially governed by the microstructural evolution induced by interactions between the produced water and mineral components. For specimens without soaking (0 day), the stress-strain curve presents a steep and highly linear elastic stage. The failure mode is characterized by a single, flat splitting surface, reflecting an intact original skeleton structure in which rigid minerals (quartz) are tightly bonded with carbonate cement (dolomite). This behavior indicates a distinctly brittle fracture mechanism. As the soaking duration increases (1-7 days), the tensile strength of the specimens gradually decreases (Fig.5). The slope of the elastic stage decreases significantly, and the post-peak stress drop becomes more gradual. The rock fractures exhibit certain deviations accompanied by slight roughening of the main splitting surface. This behavior is attributed to the initial penetration of the produced water, which preferentially dissolves dolomite and partially disrupts the cementation structure, leading to a progressive reduction in load-bearing capacity. Notably, the shale specimens soaked in produced water for 1 day display an unexpected increase in tensile strength during the Brazilian splitting test (Fig.5). A possible explanation for this phenomenon is that the slight swelling of clay minerals during the initial soaking stage reduces micro-voids at mineral interfaces, promoting tighter particle packing and enhancing the overall load-bearing capacity of the shale, while simultaneously increasing its ductile characteristics (Liu et al., 2022). When the soaking duration reaches 15 day, the tensile strength shows a secondary increase.

This behavior is possibly attributed to the secondary precipitation of carbonates (dolomite) (Fig.3), which re-cements the fractures, partially restores the structural integrity of the shale, and consequently leads to a recovery in strength (Chen et al., 2023b). At 30 day, the tensile strength decreases slightly, and

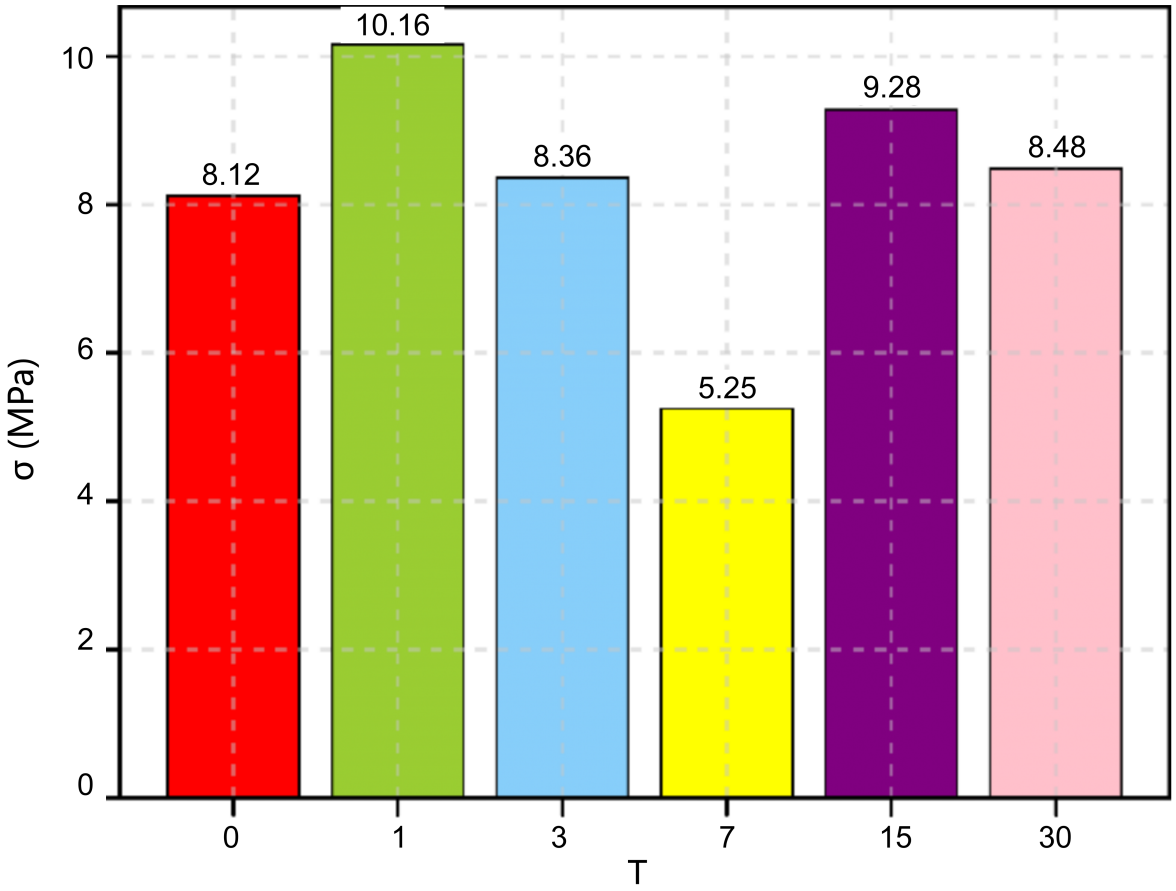


**Fig. 5** Variation in Brazilian splitting strength of different soaking times

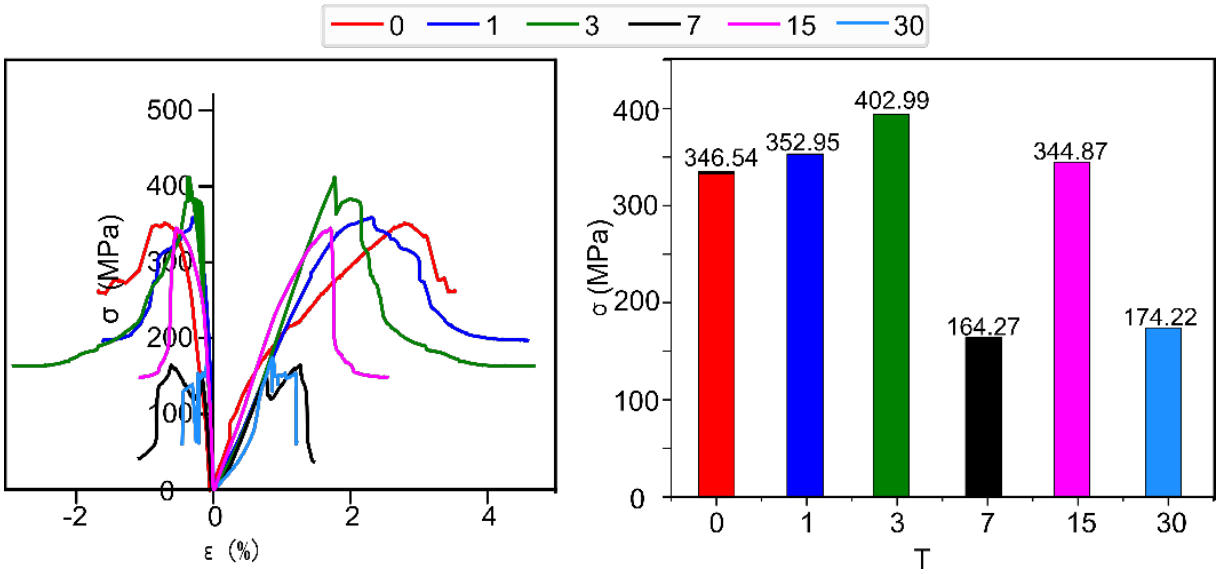


**Fig. 6** Triaxial compressive stress-strain and compressive strength of different immersion times

the failure mode evolves into a more disintegrated, fragmented pattern. A possible reason is that the cementation effect of secondary precipitation becomes limited during long-term soaking, while mild continuous dissolution or slow crack propagation leads to a slight deterioration in mechanical performance.

## 3.3 Variation in mechanical properties under triaxial compression

Fig. 6 shows the triaxial compressive stress-strain and compressive strength of different immersion times. The effect of produced water treatment on triaxial compressive strength ex-

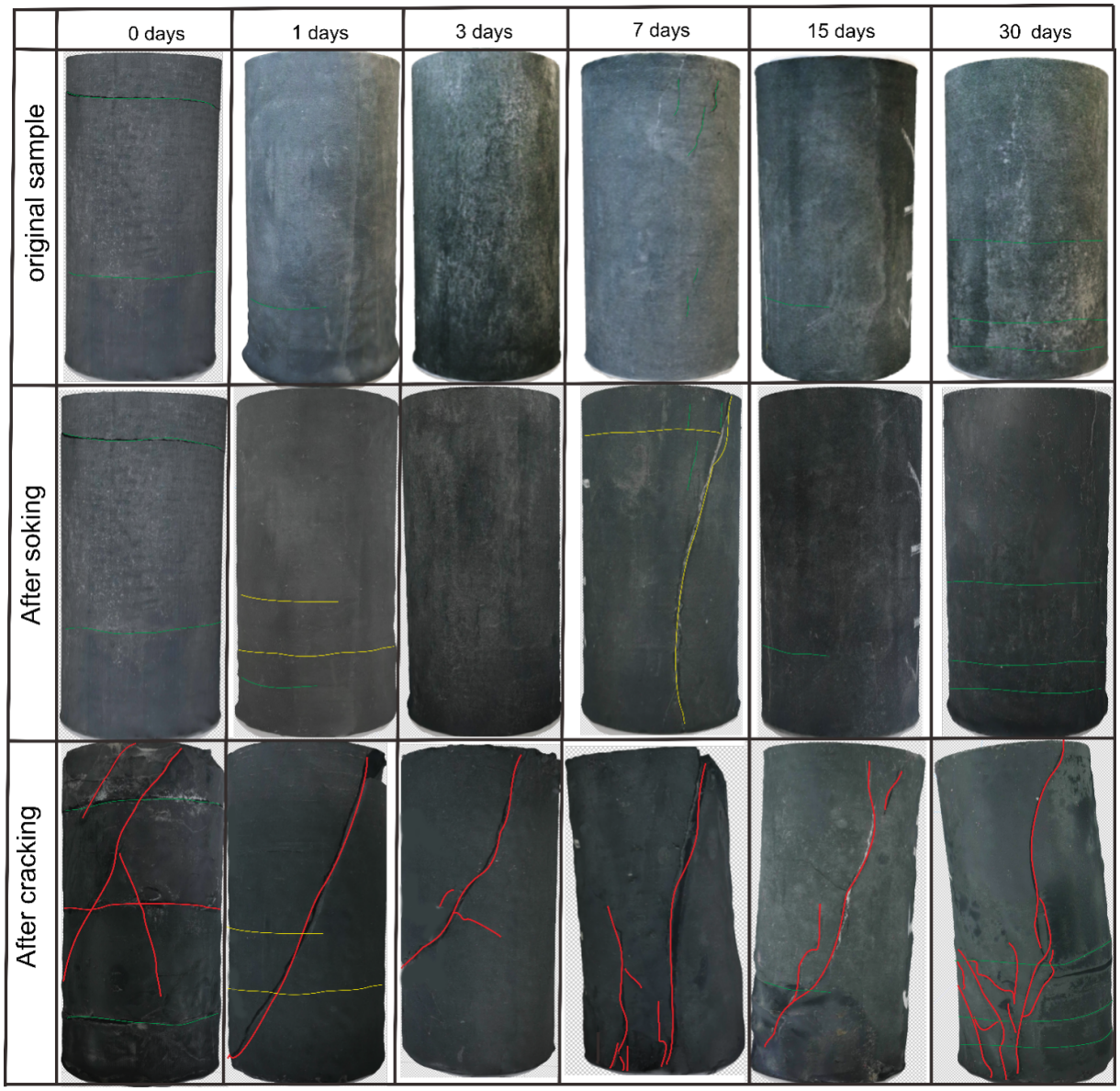


**Fig. 7** Triaxial compressive failure characteristics under different soaking times the dynamic balance of mineral dissolution and precipitation

hibits a pronounced nonlinear behavior, which can be divided into three stages: the strengthening stage (0-3 days), the degradation stage (7-15 days), and the re-stabilization stage (15-30 days). During the initial penetration of produced water (0-3 days), influenced by surface tension effects and initial reactions between the fluid and shale minerals, the local rock structure becomes denser, leading to a significant short-term increase in strength. The peak strength, $\sigma$, rises rapidly from an initial 346.54 MPa to 402.99 MPa, accompanied by a marked increase in material stiffness and overall load-bearing capacity. In the degradation stage (7-15 days), the continued swelling of minerals and the ongoing dissolution induced by active components in the produced water cause the gradual propagation of microcracks and deterioration of structural integrity, resulting in a notable decrease in triaxial compressive strength. The slope of the $\sigma-\varepsilon$ curves decreases, and the strength drops to 164.27 MPa at 7 days. Despite structural weakening, partial precipitation may fill some pores, mitigate the loss of strength and keep it above the initial level. From 15 to 30 days, the triaxial compressive strength recovers to 174.22 MPa, indicating that chemical reactions within the system approach equilibrium, and dissolution and precipitation processes gradually reach a dynamic balance. Consequently, the pore structure stabilizes, and the mechanical behavior enters the re-stabilization stage. These phenomena are primarily attributed to microstructural evolution induced by produced water-mineral interactions, where the dynamic interplay among pores, fractures, minerals, and clay leads to variations in compressive strength under different soaking durations.

Fig.7 illustrates the triaxial compressive failure characteristics under different soaking times. The evolution of failure modes is strongly coupled with the previously described mechanical properties (strength, stress-strain behavior) and mi-

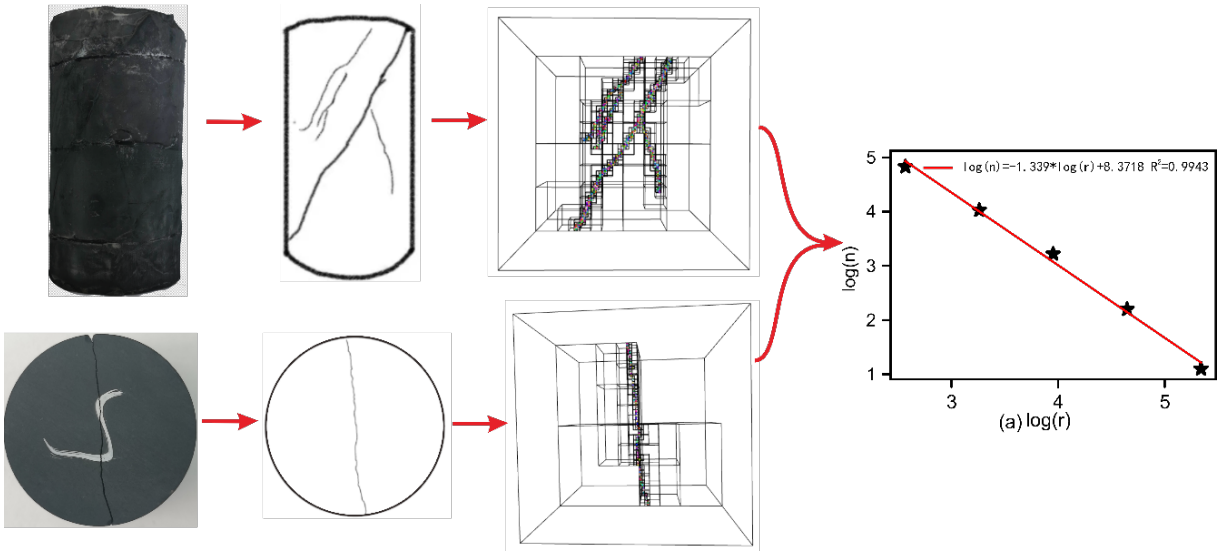


**Fig. 8** Calculation process of fractal dimension

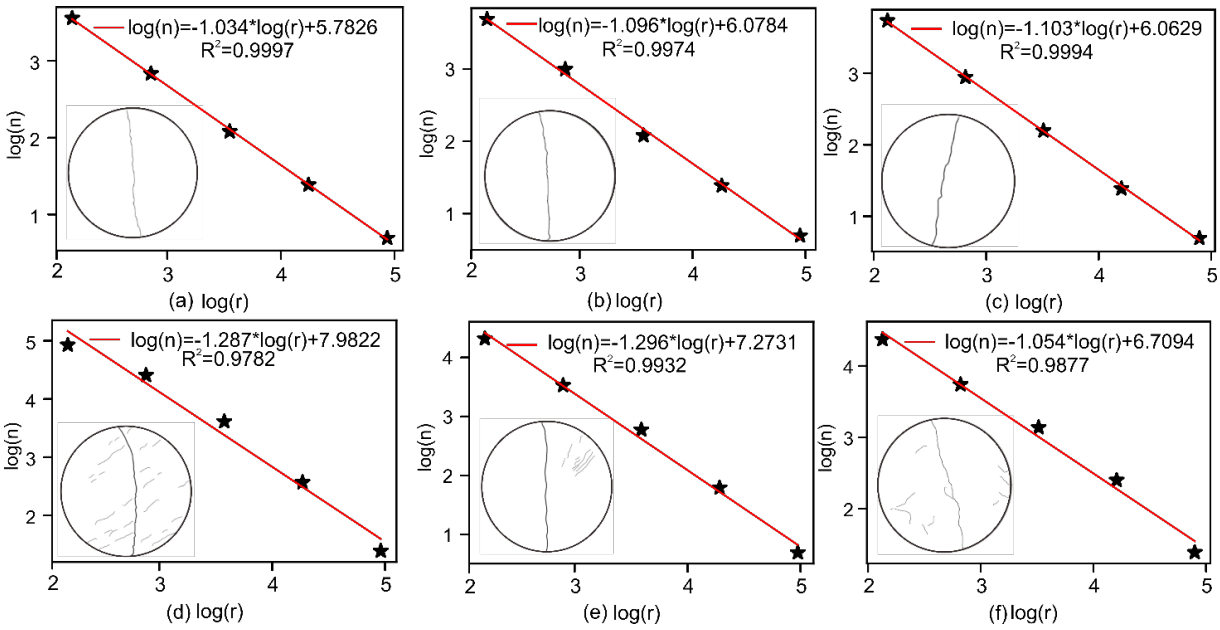


**Fig. 9** Crack morphology and fractal dimension of Brazilian split-fracture specimens of different soaking times ((a):0 day; (b):1 day; (c):3 day; (d):7 day; (e):15 day; (f):30 day)

crostructural changes. The un-soaked specimens exhibit multiple sets of parallel bedding cracks and localized fracture surfaces, but complete disintegration does not occur. Under triaxial loading, stress concentrates along the weak bedding planes, inducing brittle splitting. During the initial strengthening stage, the failure morphology is dominated by a single main crack on one side, and the overall specimen integrity remains good, with only localized cracking. This behavior results from the penetration of produced water, which fills primary pores and fractures and cements ionic particles, alleviating stress concentration and restricting crack propagation. This corresponds well with the observed increase in strength and improvement in ductility. In the mid-term degradation stage, specimens exhibit multiple through-going cracks and local fragmentation, with irregular fracture surfaces and significantly reduced structural integrity. This failure mode is attributed to microstructural deterioration: the continuous dissolution of carbonate cements such as dolomite loosens the framework, while excessive swelling of clay minerals initiates and connects micro-cracks. Although stress concentrates along multiple weak planes during triaxial compression, the overall compressive strength decreases, ultimately leading to dispersed and fragmented failure. At 15 and 30 days, the compressive strength partially recovers. The 15-day specimens display a return to a single wide main crack with significantly fewer secondary cracks. This recovery is likely due to the secondary re-cementation of major dolomite minerals, which partially fills fractures and gradually restores the overall skeleton of the specimen. At 30 days, the failure mode

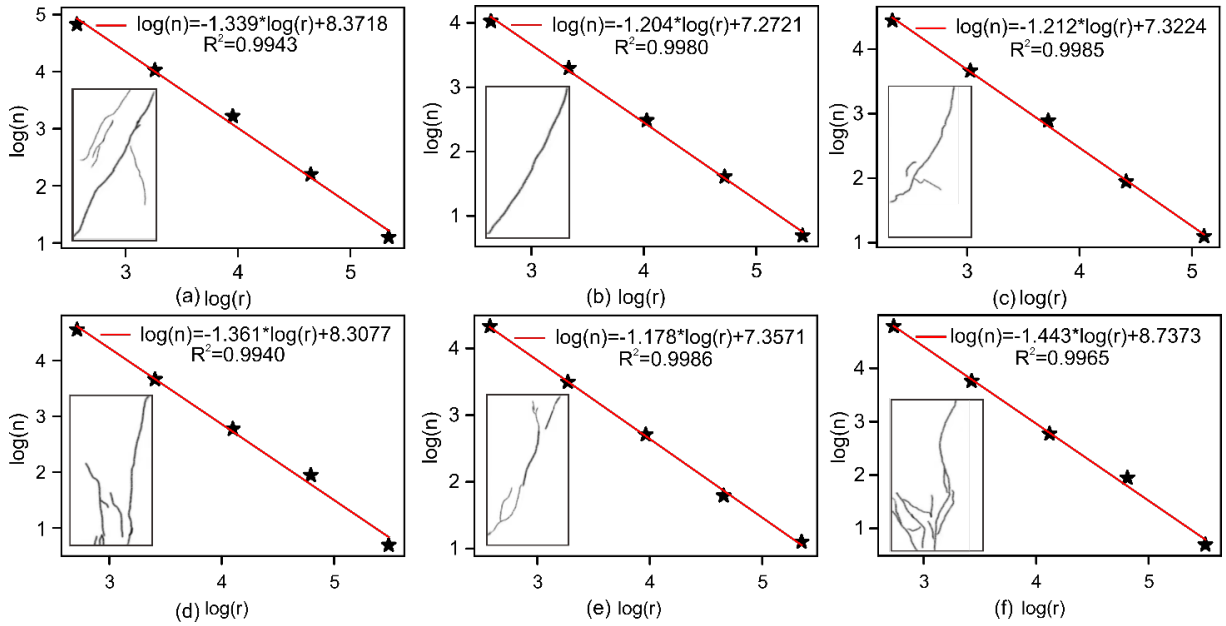


**Fig. 10** Crack morphology and fractal dimension of triaxial compression fracture specimens of different immersion durations ((a):0 day; (b):1 day; (c):3 day; (d):7 day; (e):15 day; (f):30 day)

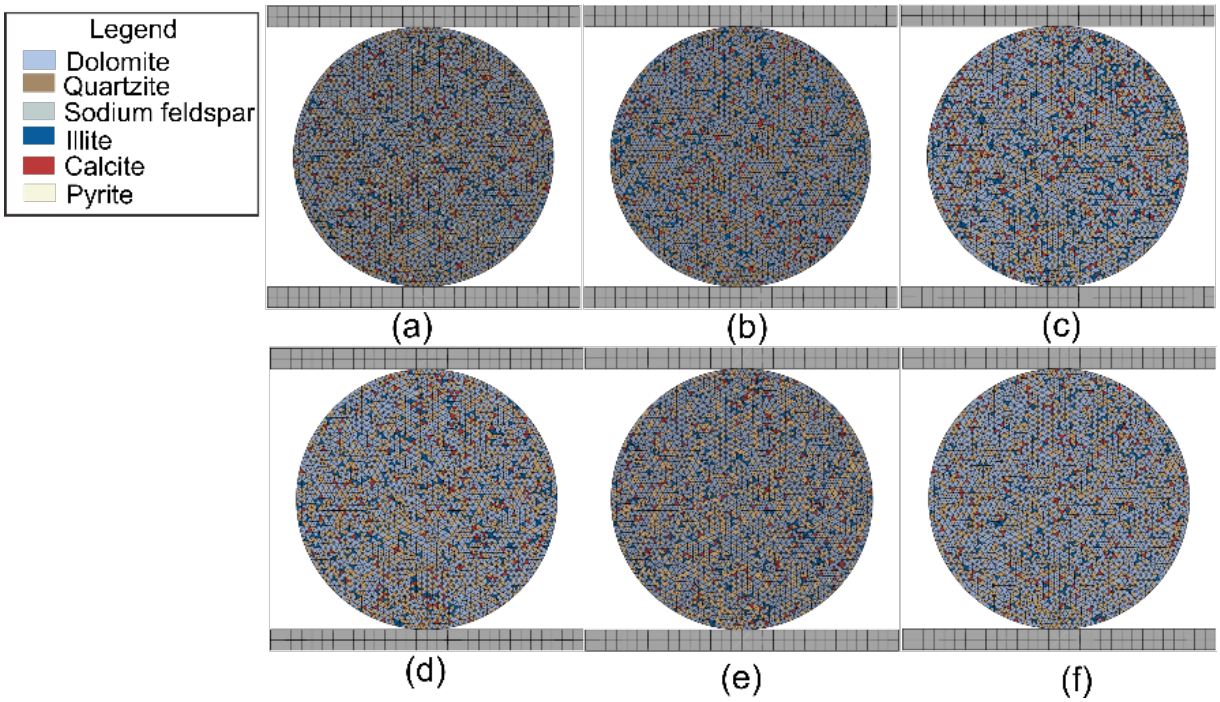


**Fig. 11** Numerical simulation model of Brazilian splitting under different soaking durations ((a):0 day; (b):1 day; (c):3 day; (d):7 day; (e):15 day; (f):30 day)

consists of one main crack accompanied by minor secondary micro-cracks. The specimen integrity and strength are slightly lower than at 15 days, and the mild deterioration is attributed to the limited cementation strength of long-term secondary precipitation and the slow propagation of pores and fractures. The evolution of these failure morphologies provides a direct visualization of the dynamic micro-processes in shale under triaxial stress and offers a basis for assessing fracture risks during the flowback stage of shale reservoirs.

## 3.4 Fractal dimension variation of crack morphology

The fracture network within rocks typically exhibits complex geometric patterns, and the distribution and morphology of these fractures directly influence the mechanical properties of the rock. The fractal dimension effectively characterizes the

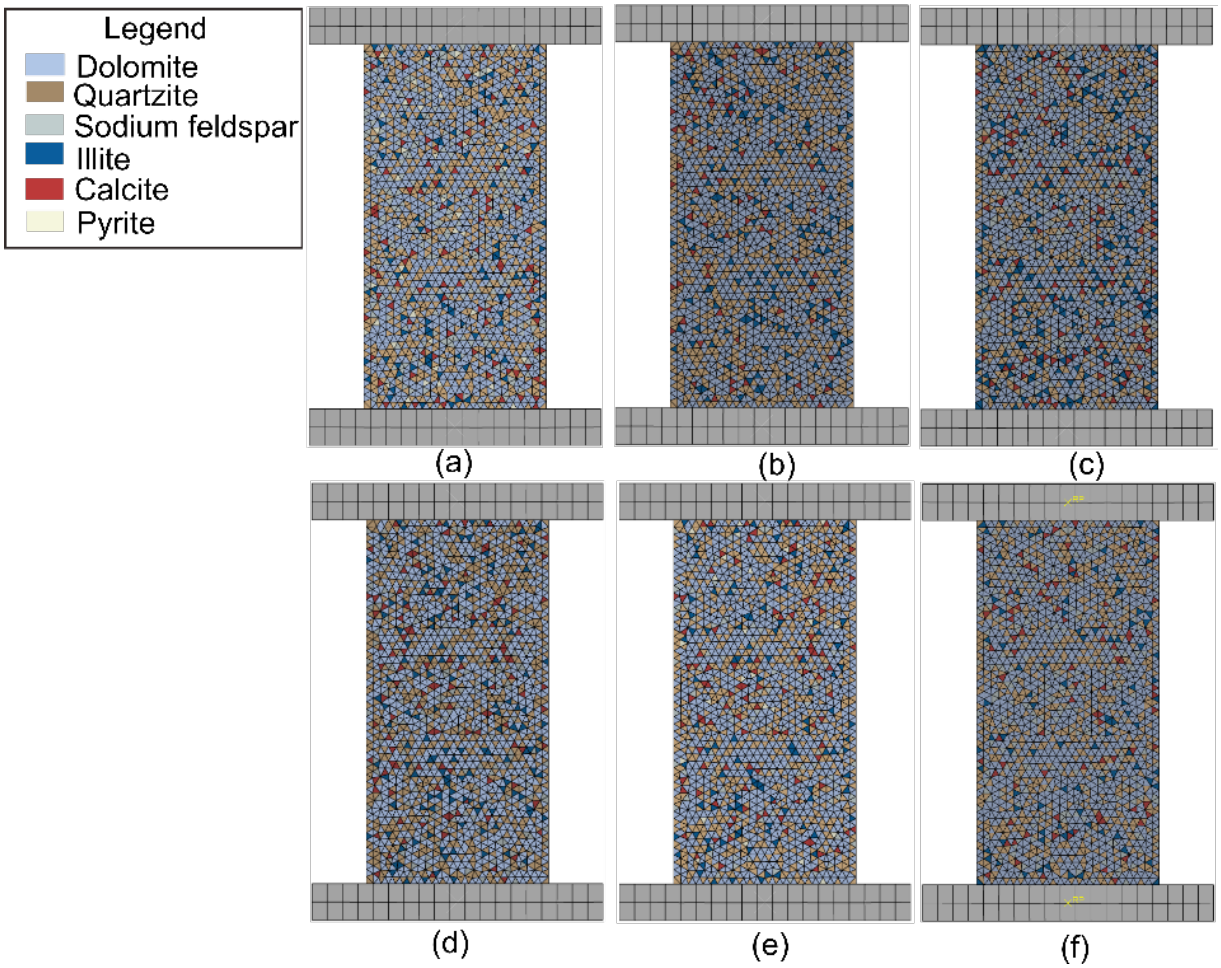


**Fig. 12** Numerical simulation model of triaxial compression under different soaking ((a):0 day; (b):1 day; (c):3 days; (d):7 day; (e):15 day; (f):30 day)

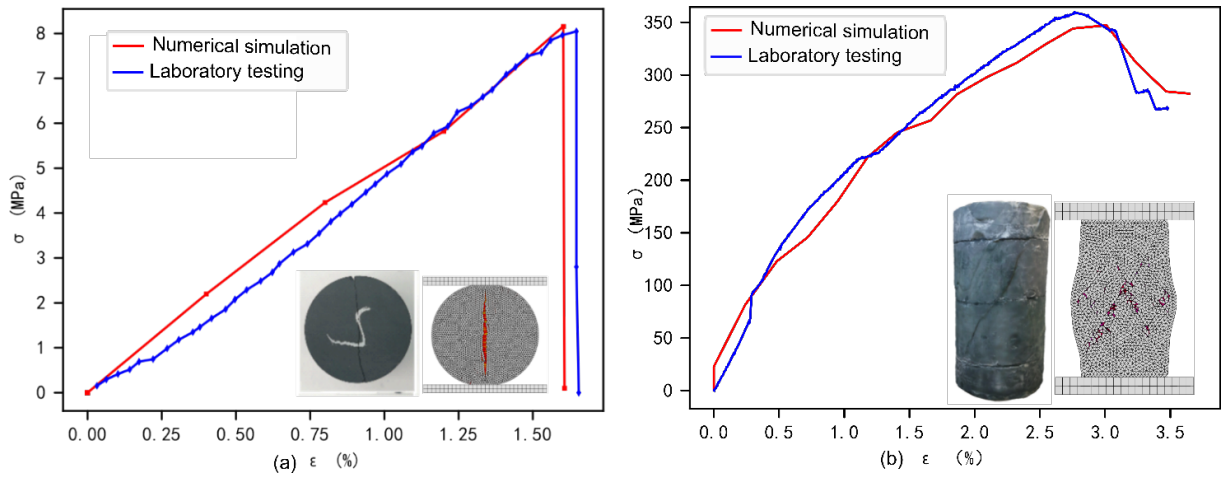


**Fig. 13** Model validation((a) Brazilian splitting;(b) triaxial compression)

self-similarity and multi-scale features of the fractures, that is, how the fracture geometry repeats at different scales (Bonnet et al., 2001). Therefore, this study aims to quantify the complexity of the fracture network by calculating the fractal dimension of the fractures in the post-failure specimen, revealing the spatial distribution characteristics of the fractures and precisely describing their morphological features. The specific procedure involves first extracting the fractures from the post-failure specimen, then binarizing the extracted fractures. A square grid is applied to the fractures using a Python script, followed by the calculation of the fractal dimension based on the number of square grid cells.

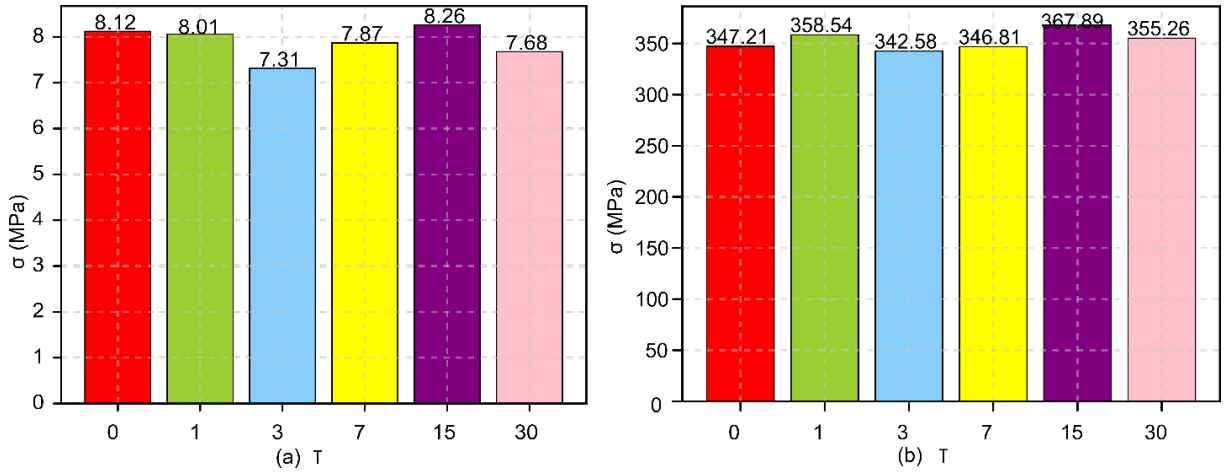


**Fig. 14** Numerical simulation of strength variation in Brazilian splitting and triaxial compression tests for shale of different mineral composition ((a) Brazilian split, (b) Triaxial compression)

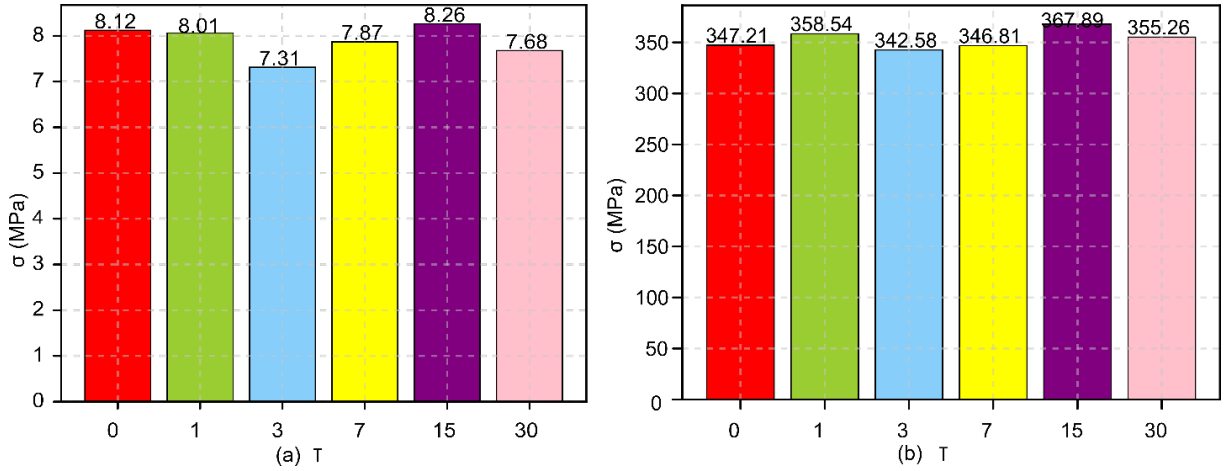


**Fig. 15** Stress evolution and crack morphology in Brazilian split numerical simulations of different mineral compositions (yellow: initial cracks; red: developed cracks)

Fig.9 and Fig.10 present the crack patterns and fractal dimensions of shale specimens under Brazilian splitting and triaxial compression. The fractal dimension of shale cracks (the absolute value of the fitted slope corresponds to D) quantitatively reflects the complexity of the crack network, with higher *D* values indicating more complex, rougher, and highly branched cracks (Sui et al., 2014). For Brazilian splitting specimens, the crack morphology evolves from a straight, simple main crack at 0 days of soaking to rough, multi-secondary microcracks at 7 days and 15 days, while at 30 days, the cracks gradually reduce.

This evolution corresponds to the Brazilian splitting failure results. For specimens soaked 0-15 days, slight carbonate dissolution and limited clay swelling weaken cementation and induce local branching, loosening the rock framework and causing strength variations. At 30 days, the dispersed crack network corresponds to moderate fluctuations, which is associated with the dynamic balance of mineral dissolution and precipitation.

In contrast, the initial fractal dimension of triaxial compression specimens is generally higher than that of Brazilian splitting specimens. This is likely due to the confinement applied during triaxial testing, which activates weak bedding planes and promotes crack branching. This phenomenon indicated that with increasing soaking time, the crack network becomes increasingly complex. After 30 day specimen exhibits a highly branched and dispersed crack network with a *D* value of 1.443, corresponding to significant carbonate dissolution and excessive clay swelling that disrupts the framework. Meanwhile, the 15-day soaked specimen shows a stable crack morphology with a moderate *D* value of 1.178, consistent with the nonlinear strength recovery observed previously and with the partial restoration of carbonate cementation that constrains excessive crack branching. Overall, during soaking, the fractal dimension of cracks is fundamentally linked to mineral mechanical interactions.

High carbonate (dolomite) content with intact cementation results in lower *D*, whereas carbonate dissolution increases *D*. Limited clay swelling slightly increases *D*, while excessive swelling leads to a significant increase in *D*.

## 4 Simulation results and discussion

Although the mechanical degradation of shale under water-

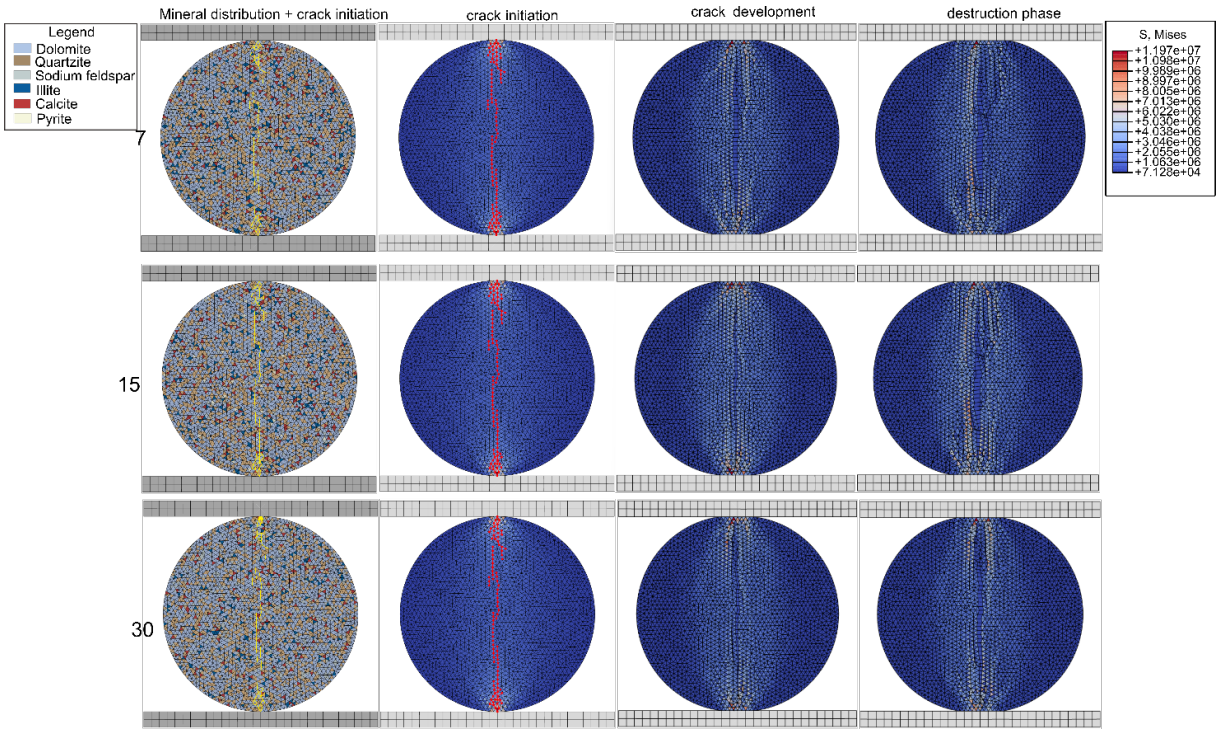


**Fig. 16** Stress evolution and crack morphology in Brazilian split numerical simulations of different mineral compositions (yellow- initial cracks; red- developed cracks)

rock interaction during Brazilian splitting and triaxial compression tests is confirmed in laboratory experiments, the degradation mechanism based on changes in mineral composition remains unverified. In this context, the construction and validation of a simulation model considering mineral variations are presented in Section 4.1. The simulation results and analysis under different mineral contents are shown in Section 4.2. Finally, a comprehensive discussion on the mechanical degradation evolution of shale based on mineral evolution and microstructure is presented in Section 4.3.

## 4.1 Simulation model calibration and scheme setting

To investigate the mechanical evolution of Shizhu shale under water-rock interaction, as influenced by changes in mineral content, this study integrates XRD testing, Brazilian splitting tests, and triaxial compression experiments. Based on the changes in mineral composition obtained from post-soaking XRD analysis and the volumetric parameters of rock specimens, a numerical simulation model for Brazilian splitting(Fig.11) and triaxial compression(Fig.12) of Shizhu shale, incorporating mineral components, is established.

A numerical simulation method is developed based on the FDEM approach, which couples DEM and FEM techniques and embeds zero-thickness cohesive elements to model mineral interfaces. This approach enables continuous-discontinuous coupling, overcoming the limitations of traditional experiments in separating independent variables and allowing direct quantification of the mechanical coupling effects among multiple mineral phases (Rougier et al., 2011; Wu et al., 2020). It facilitates full-process analysis of shale specimens during Brazilian splitting and triaxial compression simulations, capturing the complete evolution from continuous elastic deformation to discontinuous fracture (Knight et al., 2020; Cai et al., 2023). By accounting for cross-scale material interactions from the micro-scale to the macro-scale, this method provides more accurate predictions of crack propagation, material failure, and long-term rock performance under various loading conditions (Aboayanah et al., 2024). The numerical simulation model for Brazilian splitting is designed as a two-dimensional disc with a diameter of 25 mm. Rigid plates are applied at the top and bottom boundaries: the nodes at the bottom boundary are fixed in all degrees of freedom, while the top boundary is loaded using a displacement-controlled method at a constant rate of 0.002 mm/s. The force-displacement data of the top plate nodes are recorded in real time. The triaxial compression simulation model is designed similarly, as a two-dimensional rectangle with a width of 25 mm and a height of 50 mm. The boundary conditions are the same as those for the Brazilian splitting model, and the loading rate is set to a constant 0.001 mm/s. The mineral composition and mechanical properties of the minerals are listed in Table 1, and the specific model parameters are presented in Table 2.

Fig.13 show that the comparison results between indoor experiments and numerical simulations. For the Brazilian splitting test, the stress-strain curves obtained from numerical simulation (red curve) and laboratory experiments (blue curve) show a high degree of overall agreement, with good matching of peak stress and the corresponding strain. Additionally, the failure morphology of the simulated specimens, characterized by a concentrated main crack, is consistent with the actual crack distribution observed in laboratory tests, validating the model

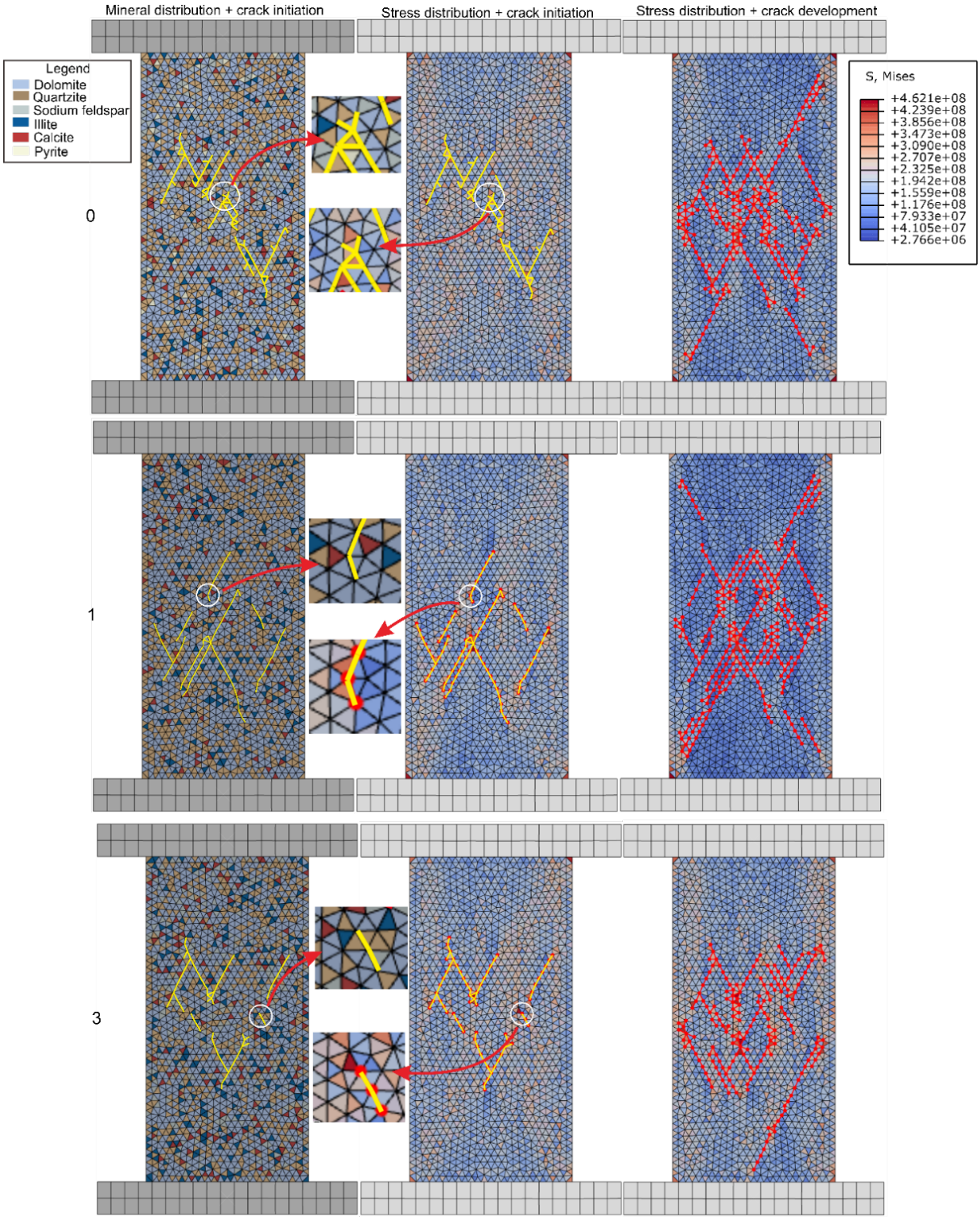


**Fig. 17** Stress evolution and crack morphology in triaxial compression numerical simulations of different mineral compositions ((yellow- initial cracks; red- developed cracks) after 0, 1, and 3 days

capability to reproduce the mechanical response and failure mode under Brazilian splitting conditions. For the triaxial compression test, the numerical simulation curves and laboratory test curves exhibit consistent trends during the elastic stage, peak stage, and post-peak softening stage. The simulated crack network and deformation characteristics also correspond well with the observed bulging and multi-crack failure patterns of the specimens after actual triaxial compression. Overall, the established numerical simulation model accurately reproduces the mechanical behavior and failure processes of shale under

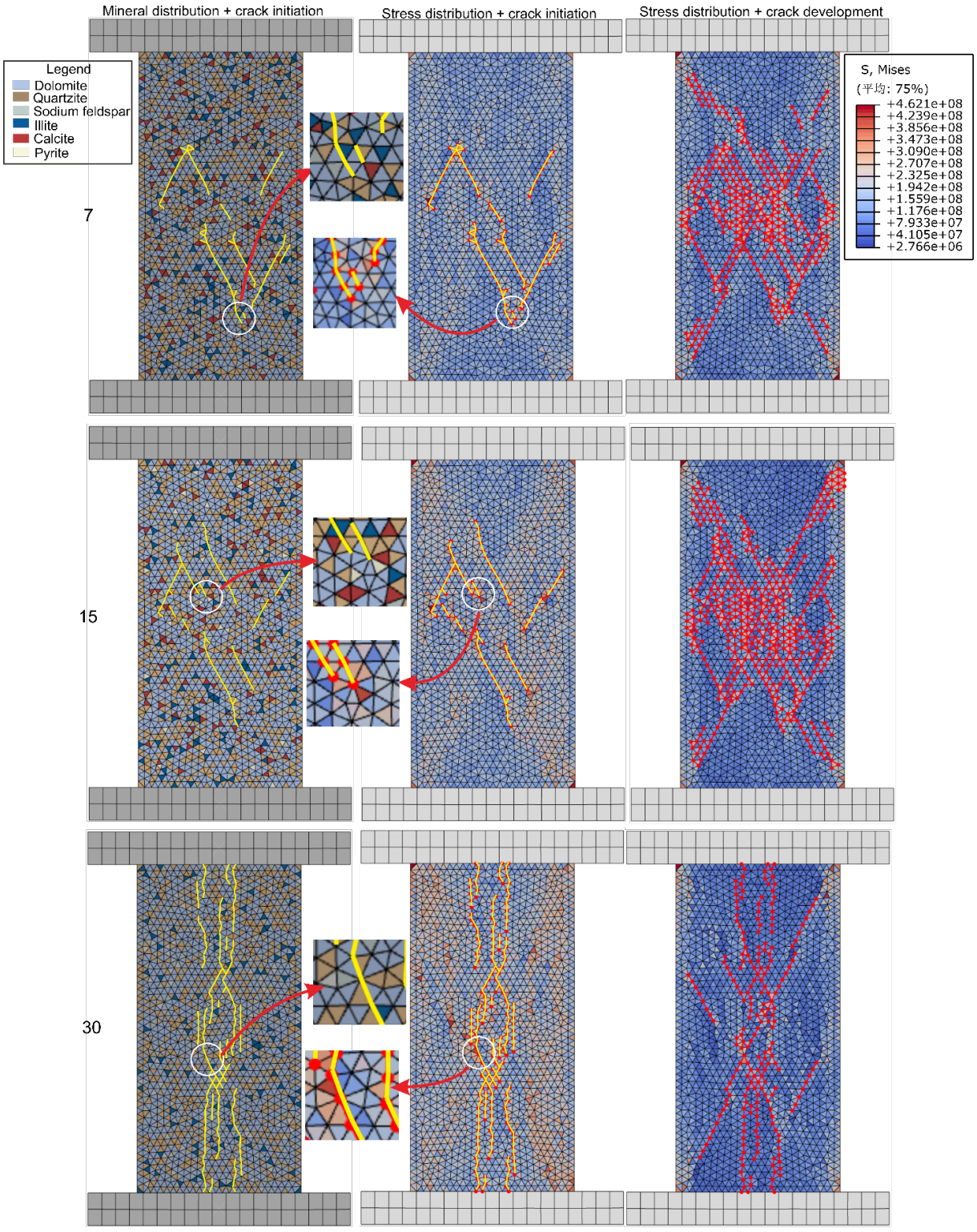


**Fig. 18** Stress evolution and crack morphology in triaxial compression numerical simulations of different mineral compositions ((yellow- initial cracks; red- developed cracks) after 7, 15 and 30 days

both Brazilian splitting and triaxial compression conditions, confirming the reliability and applicability of the model.

## 4.2 Evolution of mechanical properties under mineral changes

Fig.15 presents the numerical simulation of strength variation in Brazilian splitting and triaxial compression tests for

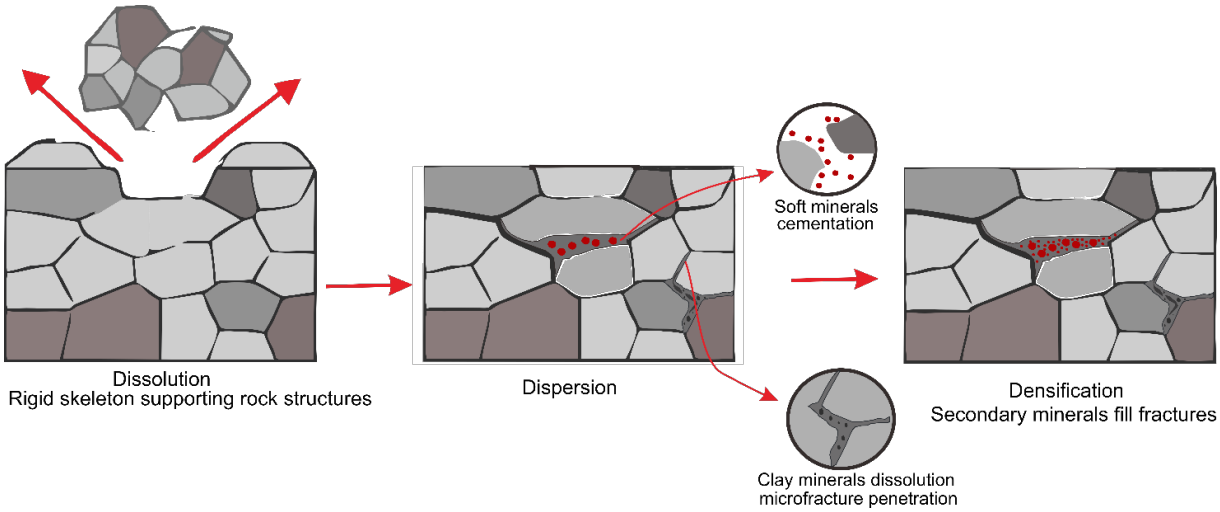


**Fig. 19** Water-rock effects on mineral dissolution and the supporting capacity of mineral frameworks

**Tab. 1** Mineral component content and mechanical parameters

| Time (days) | Dolomite (%) | Quartz (%) | Sodium feldspar (%) | Illite (%) | Calcite (%) | Pyrite (%) | Elastic modulus E(*GPa*) | Poisson's ratio ($\nu$) |
|---|---|---|---|---|---|---|---|---|
| 0 | 51.33 | 28.09 | 10.96 | 3.68 | 3.97 | 1.97 | 87 | 0.28 |
| 1 | 46.83 | 31.81 | 10.82 | 3.03 | 5.68 | 1.83 | 90 | 0.07 |
| 3 | 52.42 | 25.55 | 10.73 | 3.61 | 6.81 | 0.88 | 70 | 0.22 |
| 7 | 44.31 | 35.68 | 10.45 | 4.85 | 2.91 | 1.80 | 40 | 0.25 |
| 15 | 57.32 | 27.00 | 7.96 | 3.51 | 2.61 | 1.60 | 80 | 0.25 |
| 30 | 53.17 | 29.09 | 7.99 | 4.16 | 5.59 | 0.00 | 30 | 0.15 |

**Tab. 2** Parameters of the initial simulation model

| Parameters | Brazilian splitting Values | Triaxial compressive Values |
|---|---|---|
| Elastic modulus E (*GPa*) | 21.4 | 21.4 |
| Poisson's ratio ($\nu$) | 0.13 | 0.13 |
| Cohesive stiffness (*GPa*) | 1284 | 1070 |
| Critical displacement (*m*) | 0.001 | 0.001 |
| Tensile-shear strength ratio | 1:3 | 1:3 |
| Mineral grain size (*mm*) | 0.003 | 0.003 |

shale of different mineral composition. The simulated strength trends are consistent with the mechanical responses observed in previous experiments, confirming the reliability of the "mineral composition-microstructure-macroscopic mechanical performance" correlation mechanism. The simulations reproduce the non-monotonic strength fluctuations of shale under produced water soaking, which are fundamentally driven by the dynamic evolution of mineral mechanical properties (cementation, rigidity, plasticity, and swelling) during soaking. The initial strength (Brazilian splitting: 8.12 MPa; triaxial compression: 347.21 MPa is supported by the intact carbonate cementation (binding quartz and clay particles) and the rigid quartz framework. The stable mechanical properties of the minerals collectively maintain the baseline load-bearing capacity of the shale. After 1 day of soaking, slight dissolution of dolomite reduces its content and weakens its cementation, leading to a minor drop in tensile resistance (Brazilian splitting strength decreases slightly from 8.12 MPa to 8.01 MPa). However, the increased proportion of rigid minerals (quartz) enhances the framework support and overall stiffness in the triaxial compression simulation, resulting in a significant rise in compressive strength (to 389.52 MPa). During the 3-7 day degradation stage, the content of dolomite (and calcite) decreases significantly, while quartz content drops to its minimum. The reduction of rigid quartz contributes substantially to the observed strength decline. At 15 days, the dolomite content reaches its maximum, while the total content of clay minerals such as illite and calcite remains relatively low, leading to a recovery in strength. By 30 days, the compressive strength decreases again (355.26 MPa), possibly due to the complete loss of pyrite and the renewed increase in illite content. These results indicate that the macroscopic mechanical strength of shale is not determined by a single mineral but is the result of a dynamic balance between the strengthening effect of rigid minerals (dolomite and quartz)

and the weakening effect of soft minerals (clay minerals such as illite and calcite). The rapid variation in quartz content is particularly sensitive to strength fluctuations, whereas the high dolomite content provides a solid foundation for maintaining overall strength.

Fig.16 presents the stress evolution and crack morphology in Brazilian split numerical simulations of different mineral compositions The evolution of crack features is fundamentally governed by the dynamic mechanical interactions amon g cementing, rigid, and plastic mineral phases. Typically, the numerical simulation of Brazilian splitting produces a central vertical crack along the loading diameter. However, the heterogeneity of mineral composition significantly alters the failure pattern. When the content of rigid minerals (quartz and dolomite) is high and relatively uniformly distributed (0 days), the rock exhibits classic brittle fracture characteristics, with cracks propagating radially. As soaking time increases (1 day, 3 day, 7 day) and the content of soft minerals (illite and calcite) rises, the number of rigid/soft mineral interfaces increases, enhancing stress concentration points and local strength. This leads to more crack initiation sites, and crack propagation may be deflected or branched due to obstruction by high-hardness minerals such as dolomite. Soft, low-stiffness, and highly plastic mineral phases act as additional stress concentration points, causing cracks to deflect, branch, or even generate secondary cracks, forming more complex failure patterns (Ju et al., 2022). In particular, when dolomite content is extremely high but locally enriched or unevenly cemented (15 days), both main cracks and localized crushed zones may be observed simultaneously. By 30 days, differences in mineral composition led to peak mechanical heterogeneity, and cracks propagate along multiple mechanically weak zones, forming a network of branched cracks and widespread failure. These observations indicate that the complexity of failure modes is not solely controlled by overall mineral content but depends critically on the interaction and spatial distribution of rigid framework minerals and soft filling minerals. The latter modifies the local stress field, governing the initiation, coalescence, and eventual macroscopic propagation of micro-cracks.

Fig.16 and Fig.17 show the stress evolution and crack morphology in triaxial compression numerical simulations of different mineral compositions. At 0 days, the developed cracks (red) extend locally in a linear manner, with high-stress regions concentrated only near the cracks. As the *D* value increases (7 days, 15 days), the cracks gradually form branched structures, and the high-stress regions extend to multiple areas along the crack paths. By 30 days, the cracks exhibit a reticulated, interwoven pattern, with high-stress regions distributed throughout the specimen. The formation of these high-stress concentration points strictly corresponds to the mineral distribution. During the crack initiation stage, stress concentrations preferentially occur in regions rich in weak minerals (such as albite and illite), which have low strength and high deformability. Under loading, local stress in these regions reaches the threshold first, resulting in regional stress concentration and preferential crack initiation at clusters of low-strength minerals or at mineral interfaces. In contrast, rigid minerals such as dolomite and quartz exhibit higher mechanical strength, and cracks are less likely to initiate there. Due to gradients in mechanical parameters, deformation is locally incompatible, which also concentrates stress at interfaces between rigid minerals (dolomite, quartz) and soft minerals. As soaking time increases and further compression occurs, cracks gradually propagate, and stress concentration points dynamically reconstruct along the evolving crack paths. When cracks propagate straight through weak mineral zones, the stress at the original concentration points is released upon cracking, while new stress concentrations form at the interfaces of adjacent rigid minerals, guiding crack deflection or branching toward neighboring weak mineral zones. By the 30-day stage, the spatial distribution of mineral mechanical heterogeneity is highly dispersed, stress concentration points are ubiquitous within the specimen, and cracks continue to be guided by newly formed stress concentrations, ultimately forming a reticulated, interwoven path. Overall, with increasing soaking time, crack propagation evolves from simple linear paths to complex networked paths. The dynamic changes in mineral composition regulate the inherent differences in mineral mechanical properties within the shale and control the crack propagation path from micro- to macro-scale through single-mineral path constraints, interface-induced deflection, and the spatial complexity of mineral distribution. Quantitative characteristics of cracks in Brazilian split and triaxial compression failure specimens.

## 4.3 Comprehensive discussion

The mechanical evolution of Shizhu shale under water-rock interaction is essentially a process in which the interaction between produced water and mineral components induces microstructural reconstruction, thereby altering the evolution of macroscopic mechanical properties (Fig.18). Combined numerical simulations and quantitative fracture pattern analysis demonstrate that the mechanical property fluctuations of Shizhu shale under produced water immersion are controlled by the dynamic interactions among carbonate minerals (dolomite and calcite), silicate minerals (quartz), and clay minerals (illite). Carbonate minerals such as dolomite and calcite act as the primary cementing phases, and their dissolution-reprecipitation processes dominate the stability of the cementation system (Harrison et al., 2017; Zeng et al., 2020). In contrast, silicate minerals such as quartz exhibit extremely high mechanical stability and show only minor responses to fluid interaction, continuously serving as a rigid framework that supports the rock structure (Rybacki et al., 2015). The swelling and shrinkage behavior of clay minerals, particularly illite, directly influences intergranular pore spaces and interfacial bonding conditions (Dehghanpour et al., 2013; Liu et al., 2020; Dou et al., 2022). The proportion of hard minerals (dolomite and quartz) determines the fundamental load-bearing capacity of the shale, whereas the evolution of soft minerals (illite and calcite) governs the complexity of failure modes (Dou et al., 2022). Thus, during the initial immersion stage (0-3 days), slight dissolution of carbonate minerals and limited expansion of clay minerals jointly lead to the closure of micropores and tighter particle contacts, resulting in a short-term enhancement

of triaxial compressive strength, which increases from 111.89 MPa to 402.99 MPa. With prolonged immersion (7-15 days), continuous dissolution of carbonate minerals and progressive destruction of the cementation structure cause loosening of the rock framework and a significant reduction in strength to 164.27 MPa. By 30 days, mineral dissolution and precipitation reach a dynamic equilibrium, and the mechanical properties enter a re-stabilization stage, with strength recovering slightly to 174.22 MPa. The evolution of failure patterns further corroborates the coupled mineral mechanical mechanism ( the sudden increase in the values observed over a 15-day period may be due to variations in the test data caused by heterogeneous differences, such as internal porosity in the rock).

The fractal dimension (*D* value) quantitatively characterizes the complexity of fracture networks. For Brazilian splitting specimens, the *D* value first increases and then decreases with immersion time, consistent with the observed strength fluctuations. The highest *D* values (approximately 1.32-1.35) occur at 7-15 days, corresponding to increased fracture branching and surface roughness. At 30 days, the *D* value slightly decreases, indicating a tendency toward simplification of the fracture network. In contrast, the *D* value of triaxial compression specimens continuously increases from approximately 1.18 at the initial state to 1.44 at 30 days, suggesting that under confining pressure, the combined effects of mineral dissolution and clay swelling promote the expansion and increased complexity of fracture networks. However, due to experimental limitations, this study does not systematically investigate the coupling relationships between pore types, pore size distribution, and mechanical properties, nor does it directly monitor microstructural evolution and mineral-chemical reactions using techniques such as scanning electron microscopy (SEM). Instead, a FDEM numerical model established based on mineral composition evolution is employed to further validate the mechanical degradation mechanism. The results confirm that the macroscopic mechanical strength of shale is not governed by a single mineral phase but results from a dynamic balance between the framework-strengthening effect of hard minerals and the interface-weakening effect of soft minerals. Future studies should integrate NMR, SEM, and other advanced characterization techniques to obtain more realistic internal mineral and pore structure information, thereby further improving the predictive accuracy of numerical models and providing more comprehensive theoretical support for engineering applications.

## 5 Conclusions

This study immerses Shizhu shale in produced water and systematically conducts laboratory Brazilian splitting and triaxial compression tests. By further establishing Brazilian splitting and triaxial compression numerical models that explicitly incorporate mineral constituents, the mineralogical evolution, mechanical degradation characteristics, and underlying mechanisms of Shizhu shale under water-rock interaction are investigated in depth. The main conclusions are summarized as follows:

(1) The dynamic variation in the relative mineral contents under water–rock interaction is one of the major factors responsible for the changes in the mechanical properties of the Shizhu shale. Under the action of flowback fluid, different minerals exhibit distinct evolutionary behaviors. Quartz, which serves as the rigid framework mineral, shows strong chemical stability. In contrast, significant changes are observed in carbonate minerals such as dolomite and calcite, which display a dynamic response characterized by rapid dissolution, progressive release, and secondary precipitation. Clay minerals, particularly illite, also exhibit variation may affect inter-particle bonding and fracture complexity.

(2) The mechanical behavior of Shizhu shale under water–rock interaction shows a clear stage-dependent evolution. The strengths measured from Brazilian splitting and triaxial compression tests vary non-monotonically with soaking time and can be categorized into three successive stages: enhancement, degradation, and restabilization. This staged strength evolution closely corresponds to the coupled mineral dissolution–precipitation process and the microstructural transition from densification to collapse and finally to restabilization, demonstrating the dynamic mechanical response of shale subjected to water–rock interaction.

(3) Under water–rock interaction, the failure modes and fracture complexity of Shizhu shale in both Brazilian splitting and triaxial compression tests exhibit a systematic evolution with increasing soaking time. The Brazilian splitting specimens change from single-planar fractures to multi-branched fracture patterns, whereas the triaxial compression specimens evolve from single-fracture morphologies into interconnected network-like fracture systems. Fractal analysis further demonstrates a progressive increase in fracture complexity with soaking time. In particular, the fractal dimension of the triaxial specimens increases from 1.33 to 1.44, suggesting that carbonate dissolution and clay swelling jointly facilitate the propagation and increasing complexity of fracture networks under confinement.

(4) The FDEM model captures the main features of the stress–strain response and failure morphology, and provides a reasonable framework for interpreting the role of mineral evolution. The developed FDEM model is shown to successfully capture the stress-strain curves, peak strengths, and failure patterns of shale under Brazilian splitting and triaxial compression conditions, thereby validating its reliability. The simulation results further confirm that the macroscopic strength of shale is not governed by a single mineral phase but is controlled by a dynamic balance between the framework supporting effect provided by hard minerals (dolomite and quartz) and the interface- weakening effect induced by soft minerals (illite and calcite). The mechanical evolution of shale under water-rock interaction is therefore interpreted as a process in which the dynamic interactions between produced water and mineral constituents (dissolution, precipitation, and swelling) induce microstructural reconstruction (pore-fracture evolution and changes in inter-particle bonding), which in turn drives the staged evolution of macroscopic mechanical properties (strengthening-degradation-restabilization). The revealed mechanism provides essential theoretical support for engineering stability assessment and parameter optimization in shale

reservoir development.

## Acknowledgements

This research is financially supported by the National Science and Technology Major Project "Technology for Enhanced Oil Recovery and Efficient Development in Large Oil and Gas Fields along the Belt and Road Region" (2025ZD1406404), the National Natural Science Foundation of China (U24B2035, 52404102), the Natural Science Foundation of Hubei Province (2024AFD374), the Youth Project from the Hubei Research Center for Basic Disciplines of Earth Sciences (HRCES-202407), and the Guangdong Provincial Key Laboratory of Deep Earth Sciences and Geothermal Energy Exploitation and Utilization (ESGEEU-2025-05).

## Conflict of interest

The authors declare no competing interest.



## References

Aboayanah KR, Abdelaziz A, Haile BF, et al. 2024. Evaluation of damage stress thresholds and mechanical properties of granite: New insights from digital image correlation and GB-FDEM. *Rock Mechanics and Rock Engineering*, **57**(7):4679–4706. doi:10.1007/s00603-024-03789-7.

Al-Shafi M, Massarweh O, Abushaikha A S, et al. 2023. A review on underground gas storage systems: Natural gas, hydrogen and carbon sequestration. *Energy Reports*, **9**:6251–6266. doi:10.1016/j.egyr.2023.05.236.

Bonnet E, Bour O, Odling NE, et al. 2001. Scaling of fracture systems in geological media. *Reviews of Geophysics*, **39**(3):347–383. doi:10.1029/1999RG000074.

Bourg I C, Ajo-Franklin J B. 2017. Clay, water, and salt: Controls on the permeability of fine-grained sedimentary rocks. *Accounts of Chemical Research*, **50**(9):2067–2074. doi:10.1021/acs.accounts.7b00261.

Cai WB, Gao K, Ai SG, et al. 2023. Implementation of extrinsic cohesive zone model (eczm) in 2d finite-discrete element method (FDEM) using node binding scheme. *Computers and Geotechnics*, **159**:105470. doi:10.1016/j.compgeo.2023.105470.

Cai X, Zhou ZL, Liu KW, et al. 2019. Water-weakening effects on the mechanical behavior of different rock types: Phenomena and mechanisms. *Applied Sciences*, **9**(18):3782. doi:10.3390/app9204450.

Chen XF, Eichhubl P, Olson JE, et al. 2019. Effect of water on fracture mechanical properties of shales. *Journal of Geophysical Research: Solid Earth*, **124**(3):2428–2444. doi:10.1029/2018JB016479.

Chen XD, Ou WB, Fukuda D, et al. 2023. Three-dimensional modelling on the impact fracture of glass using a GPGPU-parallelised FDEM. *Engineering Fracture Mechanics*, **277**:108929. doi:10.1016/j.engfracmech.2022.108929.

Chen Y, Cao P, Mao DW, et al. 2014. Morphological analysis of sheared rock with water–rock interaction effect. *International Journal of Rock Mechanics and Mining Sciences*, **70**(Complete):264–272. doi:10.1016/j.ijrmms.2014.05.002.

Chen ZL, Shi HZ, Xiong C, et al. 2023. Effects of mineralogical composition on uniaxial compressive strengths of sedimentary rocks. *Petroleum Science*, **20**(5):3062–3073. doi:10.1016/j.petsci.2023.03.028.

Dehghanpour H, Lan Q, Saeed Y, et al. 2013. Spontaneous imbibition of brine and oil in gas shales: Effect of water adsorption and resulting microfractures. *Energy & Fuels*, **27**(6):3039–3049. doi:10.1021/ef4002814.

Deng PH, Liu QS, Lu HF, et al. 2024. A FDEM study on the mechanical properties and failure behavior of soft-hard interbedded rocks considering the size effect. *Engineering Fracture Mechanics*, **310**:110489. doi:10.1016/j.engfracmech.2024.110489.

Dou FK, Hou P, Jia ZR, et al. 2022. Effect of clay minerals on tensile failure characteristics of shale. *ACS Omega*, **7**(28):24219–24230. doi:10.1021/acsomega.2c01344.

Erguler ZA, Ulusay R. 2009. Water-induced variations in mechanical properties of clay-bearing rocks. *International Journal of Rock Mechanics and Mining Sciences*, **46**(2):355–370. doi:10.1016/j.ijrmms.2008.07.002.

Fukuda D, Liu HY, Zhang QB, et al. 2021. Modelling of dynamic rock fracture process using the finite-discrete element method with a novel and efficient contact activation scheme. *International Journal of Rock Mechanics and Mining Sciences*, **138**:104645. doi:10.1016/j.ijrmms.2021.104645.

Guo W, Zhang B, Liang Y, et al. 2022. Improved method and practice for site selection of underground gas storage under complex geological conditions. *Journal of Natural Gas Science and Engineering*, **108**:104813. doi:10.1016/j.jngse.2022.104813.

Harrison AL, Jew AD, Dustin MK, et al. 2017. Element release and reaction-induced porosity alteration during shale-hydraulic fracturing fluid interactions. *Applied Geochemistry*, **82**:47–62. doi:10.1016/j.apgeochem.2017.05.001.

Ju MH, Li XF, Li X, et al. 2022. A review of the effects of weak interfaces on crack propagation in rock: From phenomenon to mechanism. *Engineering Fracture Mechanics*, **263**:108297. doi:10.1016/j.engfracmech.2022.108297.

Knight EE, Rougier E, Lei Z, et al. 2020. Hoss: An implementation of the combined finite-discrete element method. *Computational Particle Mechanics*, **7**(5):765–787. doi:10.1007/s40571-020-00349-y.

Lai J, Wang GW, Wang ZY, et al. 2018. A review on pore structure characterization in tight sandstones. *Earth-Science Reviews*, **177**:436–457. doi:10.1016/j.earscirev.2017.12.003.

Li G. 2023. Analytical estimation of cohesive parameters for a bilinear traction-separation law in dcb mode i loading. *Journal of Mechanics of Materials and Structures*, **18**(3):293–317. doi:10.2140/jomms.2023.18.293.

Li Y, Jiang Y, Jiang W, et al. 2025. Sensitivity study of the F-DEM model of brazilian splitting for weiyuan shale considering mineral components. *ACS Omega*, **10**(39):45496–45515. doi:10.1021/acsomega.5c04555.

Liu JJ, Yang CH, Song R, et al. 2025. Advances of geological storage engineering and technology. *GeoStorage*, **1**(1):1–26. doi:10.46690/gs.2025.01.01.

Liu KR, Sheng JJ, Zhang ZK. 2020. A simulation study of the effect of clay swelling on fracture generation and porosity change in shales under stress anisotropy. *Engineering Geology*, **278**:105829. doi:10.1016/j.enggeo.2020.105829.

Liu WL, Ji F, Liu PE, et al. 2024. Study on the microstructure evolution and strength deterioration of powder crystal dolomite under dissolution. *Water*, **16**(14):1989. doi:10.3390/w16141989.

Liu WL, Liu PG, Xu HH, et al. 2022. Study on the microstruc-

ture evolution and strength damage mechanism of dolomite under dissolution condition. *Sustainability*, **14**(18):11447. doi:10.3390/su141811447.

Lyu Q, Long XP, Ranjith PG, et al. 2018. Experimental investigation on the mechanical behaviours of a low-clay shale under water-based fluids. *Engineering Geology*, **233**:124–138. doi:10.1016/j.enggeo.2017.12.002.

Mao LJ, Cui WY, Chen M, et al. 2025. Solidified tailings-contaminated sludge as an anti-seepage material for solid waste landfills: Mechanical characteristics and microscopic mechanisms. *GeoStorage*, **1**(2):171–179. doi:10.46690/gs.2025.02.06.

Pang J, Wu T, Yu X, et al. 2025. The effect of water–rock interaction on shale reservoir damage and pore expansion. *Processes*, **13**(5):1265. doi:10.3390/pr13051265.

Rougier E, Knight EE, Sussman AJ, et al. 2011. The combined finite-discrete element method applied to the study of rock fracturing behavior in 3d. *45th U.S. Rock Mechanics / Geomechanics Symposium, San Francisco, California, June 2011*, ARMA-11-517.

Rybacki E, Reinicke A, Meier T, et al. 2015. What controls the mechanical properties of shale rocks?–part i: Strength and young's modulus. *Journal of Petroleum Science and Engineering*, **135**:702–722. doi:10.1016/j.petrol.2015.10.028.

Shen WJ, Li XZ, Cihan A, et al. 2019. Experimental and numerical simulation of water adsorption and diffusion in shale gas reservoir rocks. *Advances in Geo-Energy Research*, **3**(2):165–174. doi:10.26804/ager.2019.02.06.

Song R, Chen JY, Zou SJ, et al. 2026. Review on carbon sequestration in salt rock caverns: Application, theory and potentials in china. *GeoStorage*, **2**(1):1–13. doi:10.46690/gs.2026.01.01.

Sun C, Zheng H, Liu WD, et al. 2020. Study on dynamic propagation of hydraulic fractures in enhanced thermal reservoir. *Engineering Fracture Mechanics*, **236**:107207. doi:10.1016/j.engfracmech.2020.107207.

Sui LL, Yang YM, Ju Y, et al. 2014. Fractal description of rock fracture behavior. *Mechanics in Engineering*, **36**(6):753–756,746. doi:10.6052/1000-0879-14-025.

Taleghani AD, Gonzalez-Chavez M, Yu H, et al. 2018. Numerical simulation of hydraulic fracture propagation in naturally fractured formations using the cohesive zone model. *Journal of Petroleum Science and Engineering*, **165**:42–57. doi:10.1016/j.petrol.2018.01.063.

Taleghani AD, Gonzalez M, Shojaei A. 2016. Overview of numerical models for interactions between hydraulic fractures and natural fractures: Challenges and limitations. *Computers and Geotechnics*, **71**:361–368. doi:10.1016/j.compgeo.2015.09.009.

Wilson MJ. 2020. Dissolution and formation of quartz in soil environments: A review. *Soil Science Annual*, **71**(2):99–110. doi:10.37501/soilsa/122398.

Wu MY, Wang WS, Shi D, et al. 2021. Improved box-counting methods to directly estimate the fractal dimension of a rough surface. *Measurement*, **177**:109303. doi:10.1016/j.measurement.2021.109303.

Wu Z, Ji X, Liu Q, et al. 2020. Study of microstructure effect on the nonlinear mechanical behavior and failure process of rock using an image-based-FDEM model. *Computers and Geotechnics*, **121**:103480. doi:10.1016/j.compgeo.2020.103480.

Xia BW, Zhang XG, Ma ZK, et al. 2024. Numerical simulation of multiple hydraulic fracture propagation in heterogeneous coal reservoirs based on combined finite-discrete element method. *Frontiers in Earth Science*, **12**:1411129. doi:10.3389/feart.2024.1411129.

Zeng LP, Lu YH, Maskari NSA, et al. 2020. Interpreting micromechanics of fluid-shale interactions with geochemical modelling and disjoining pressure: Implications for calcite-rich and quartz-rich shales. *Journal of Molecular Liquids*, **319**:114117. doi:10.1016/j.molliq.2020.114117.

Zhang RH, Hu SM, Zhang XT, et al. 2007. Dissolution kinetics of dolomite in water at elevated temperatures. *Aquatic Geochemistry*, **13**(4):309–338. doi:10.1007/s10498-007-9022-z.

Zhang YJ, Zhang DP, Feng GR, et al. 2024. Characteristics of penetration strength and fracture features under nonuniform stress field around borehole surrounding rock. *ACS Omega*, **9**(24):26168–26182. doi:10.1021/acsomega.4c01661.

Zheng Y, Yan C, Zheng H. Modified joint element constitutive model for FDEM to simulate the nonlinear mechanical behavior of rocks. *Computers and Geotechnics*, **164**:105831. doi:10.1016/j.compgeo.2023.105831.

Zou SM, Zhang YH, Ma L, et al. 2024. Revealing subsurface dynamics: Imaging techniques for optimizing underground energy storage. *Advances in geo-energy research*, **12**(1):1–7. doi:10.46690/ager.2024.04.01.